



NOAA Technical Memorandum, OAR AOML-96

**THE SEA-AIR CO₂ FLUX IN THE NORTH ATLANTIC ESTIMATED FROM
SATELLITE AND ARGO PROFILING FLOAT DATA**

H. Lueger
R. Wanninkhof
A. Olsen
J. Triñanes
T. Johannessen
D.W.R. Wallace
A. Körtzinger

Atlantic Oceanographic and Meteorological Laboratory
Miami, Florida

August 2008

noaa

**NATIONAL OCEANIC AND
ATMOSPHERIC ADMINISTRATION**

**Office of Oceanic and
Atmospheric Research**

NOAA Technical Memorandum, OAR-AOML-96

**THE SEA-AIR CO₂ FLUX IN THE NORTH ATLANTIC ESTIMATED FROM
SATELLITE AND ARGO PROFILING FLOAT DATA**

Heike Lueger
University of Miami/Cooperative Institute for Marine and Atmospheric Studies,
Miami, Florida

Rik Wanninkhof
NOAA/Atlantic Oceanographic and Meteorological Laboratory, Miami, Florida

Are Olsen
University of Bergen/Geophysical Institute and Bjerknes Centre for Climate Research,
Bergen, Norway

Joaquin Triñanes
University of Santiago de Compostela/Technological Research Institute,
Santiago de Compostela, Spain

Truls Johannessen
University of Bergen/Geophysical Institute, Bergen, Norway

Douglas W.R. Wallace
Leibniz-Institut für Meereswissenschaften, Kiel, Germany

Arne Körtzinger
Leibniz-Institut für Meereswissenschaften, Kiel, Germany

August 2008



**UNITED STATES
DEPARTMENT OF COMMERCE**

**Carlos M. Gutierrez
Secretary**

**NATIONAL OCEANIC AND
ATMOSPHERIC ADMINISTRATION**

**VADM Conrad C. Lautenbacher, Jr.
Undersecretary for Oceans and
Atmosphere/Administrator**

Office of Oceanic and
Atmospheric Research

Dr. Richard W. Spinrad
Assistant Administrator

Disclaimer

NOAA does not approve, recommend, or endorse any proprietary product or material mentioned in this document. No reference shall be made to NOAA or to this document in any advertising or sales promotion which would indicate or imply that NOAA approves, recommends, or endorses any proprietary product or proprietary material herein or which has as its purpose any intent to cause directly or indirectly the advertised product to be used or purchased because of this document.

The findings and conclusions in this report are those of the authors and do not necessarily represent the views of the funding agency.

Table of Contents

List of Figures	iv
List of Tables	vi
List of Acronyms	vii
Abstract	1
1. Introduction	1
2. Hydrographic Setting	2
3. Data and Methods	3
3.1 $f\text{CO}_2$ _{sw} Data	3
3.2 Satellite and Argo Data	6
3.3 CO_2 Flux Calculation based on Algorithms ($F_{2 \times 2}$)	8
3.4 CO_2 Flux Calculation based on Cruises ($F_{4 \times 5}$)	8
3.5 CO_2 Flux Calculation based on Climatology ($F_{4 \times 5}$ climatol)	9
3.6 Satellite Chlorophyll Data	9
4. Algorithms	11
4.1 North Atlantic Drift Province (NADR)	11
4.2 Atlantic Arctic Province (ARCT)	13
4.3 Gulf Stream Province (GFST)	14
5. Results and Discussion	15
5.1 Estimates of Seawater $f\text{CO}_2$ _{sw}	15
5.2 Seasonal Maps of $\Delta f\text{CO}_2$ and CO_2 Flux	17
5.3 Source and Sink Patterns of CO_2 in the North Atlantic based on the Different Approaches	19
6. Conclusions	23
7. Acknowledgments	24
8. References	25

List of Figures

Figure 1.	VOS cruises (gray lines) and boundaries of the three provinces that were used in the analysis. The gray circles denote the $2^\circ \times 2^\circ$ grids, while the open white circles display the Takahashi <i>et al.</i> (2002) grid ($4^\circ \times 5^\circ$). ARCT: Atlantic Arctic province; NADR: North Atlantic Drift; GFST: Gulf Stream. The overlapping $2^\circ \times 2^\circ$ grids between the NADR and GFST provinces were compared and yielded nearly identical flux results (not shown).	3
Figure 2.	Difference between SST observed onboard the VOS (SST_{TSG}) and SST retrieved from AVHRR (SST_{AVHRR}) versus the distance between the satellite and ship data ($n = 24,382$).	6
Figure 3.	Comparison of the residuals and predicted $fCO_{2\ sw}$ data in the NADR province. The predicted $fCO_{2\ sw}$ data were retrieved from equation 8 by using temperature, mixed layer depth data (source: AVHRR/Argo), and position information. Also shown is the mean difference which is $-0.1\ \mu atm$ (black bar on the right).....	12
Figure 4.	Comparison of the residuals and predicted $fCO_{2\ sw}$ data in the ARCT province. The predicted $fCO_{2\ sw}$ data were retrieved from equation 9 by using mixed layer depth data (source: Argo), SST (source: AVHRR), and position information. Also shown is the mean difference which is $0.00\ \mu atm$ (black bar on the right).	13
Figure 5.	Comparison of the measured and the predicted $fCO_{2\ sw}$ data for the GFST province. The predicted $fCO_{2\ sw}$ data were retrieved by using equation 10 and AVHRR temperature, Argo mixed layer depth data, and position information for the algorithm data. Also shown is the mean difference which is $-0.12\ \mu atm$ (black bar on the right)..	15
Figure 6.	Seasonal ΔfCO_2 across the North Atlantic. The ΔfCO_2 data were calculated from the $2^\circ \times 2^\circ$ dataset which uses province-specific algorithms to predict the seawater fCO_2 . The rectangles show the province-specific margins.....	18
Figure 7.	Seasonal CO_2 fluxes across the North Atlantic in 2002. The fluxes were calculated from the $2^\circ \times 2^\circ$ dataset which uses the province-specific algorithms to predict the seawater fCO_2 . The rectangles show the province-specific margins.....	19

Figure 8.	Comparison of the monthly ΔfCO_2 within all three provinces using the $2^\circ \times 2^\circ$ proxy algorithm CO_2 (light gray), $4^\circ \times 5^\circ$ bin-averaged cruise (white), and $4^\circ \times 5^\circ$ climatological (black) fCO_2 data within the three provinces.....	20
Figure 9.	Comparison of the monthly CO_2 fluxes within all three provinces using the $2^\circ \times 2^\circ$ proxy CO_2 (light gray), $4^\circ \times 5^\circ$ bin-averaged cruise (white), and $4^\circ \times 5^\circ$ climatological (black) fCO_2 data within the three provinces.....	21

List of Tables

Table 1. Cruises on Volunteer Observing Ships that were used in this work. The validation cruises are not shown.....	4
Table 2. Data sources used to compute the CO ₂ flux for the three approaches. The climatology by Takahashi <i>et al.</i> (2002) for the virtual year 1995 is normalized to 2002.....	7
Table 3. Comparison of the statistical results in the spring (April-June) for predicted fCO _{2 sw} data within the three provinces (NADR, ARCT, GFST) retrieved by regression analysis. Predictors are AVHRR SST, Argo mixed layer depth, and position including and excluding MODIS chlorophyll within the algorithm. RMS: root mean square error (random error); r ² : regression coefficient; mean residual difference: average of the residuals (=bias); data points: number of data points used for algorithm.	10
Table 4. Statistical results for predicted fCO _{2 sw} data within three provinces (NADR, ARCT, GFST) retrieved by regression analysis. Predictors are AVHRR SST and Argo mixed layer depth. RMS: root mean square error (random error); r ² : regression coefficient; mean residual difference: average of the residuals (=bias); data points: number of data used for algorithm; validation: independent data used to test the algorithms.	12
Table 5. Annual CO ₂ flux calculated from three approaches for the year 2002. CO ₂ proxy: algorithms have been used to calculate the flux at a 2° × 2° resolution (F _{2x2}); cruise extrapolation: all VOS cruises were bin averaged to a 4° × 5° grid and then the flux was calculated (F _{4x5}); Takahashi <i>et al.</i> (2002): climatological ΔfCO ₂ were used for the flux calculation based on the 4° × 5° grids (F _{4x5/climatology}). The details of the flux calculation are described in the text.....	22

List of Acronyms

AOML	Atlantic Oceanographic and Meteorological Laboratory
ARCT	Atlantic Arctic gyre
AVHRR	Advanced Very High Resolution Radiometer
BATS	Bermuda Atlantic Time Series
DIC	Dissolved inorganic carbon
GFST	Gulf Stream
MLD	Mixed layer depth
MODIS	Moderate Resolution Imaging Spectroradiometer
NADR	North Atlantic Drift
NASA	National Aeronautics and Space Administration
NCAR	National Center for Atmospheric Research
NCEP	National Centers for Environmental Prediction
NOAA	National Oceanic and Atmospheric Administration
PODAAC	Physical Oceanography Distributed Active Archive Center
QuikSCAT	Quick scatterometer
RMS	Root mean square
SeaWiFS	Sea-viewing Wide Field of View Scanner
SLP	Sea level pressure
SSS	Sea surface salinity
SST	Sea surface temperature
VOS	Volunteer observing ship

The Sea-Air CO₂ Flux in the North Atlantic Estimated from Satellite and Argo Profiling Float Data

Abstract

To improve the spatial and temporal resolution of sea-air carbon dioxide (CO₂) flux estimates in the mid-latitude North Atlantic Ocean (30°N-63°N), empirical relationships were derived between the measured fugacity of CO₂ in surface water (fCO_{2 sw}), sea surface temperature (SST), and the mixed layer depth (MLD). Satellite chlorophyll was unsuccessful as a predictive parameter. The algorithms for fCO_{2 sw} predictions were developed using Advanced Very High Resolution Radiometer (AVHRR) satellite SST and MLD data obtained from Argo floats. The root mean square (RMS) difference between the algorithms and fCO_{2 sw} data was 9-10 μatm with a precision, determined from independent data, of 9-11 μatm. This precision is close to that necessary to constrain the sea-air flux in the mid-latitude North Atlantic Ocean to 0.1 Pg C yr⁻¹. The algorithms were applied on high-resolution SST and MLD data to yield fCO_{2 sw} proxy data for the entire region. The proxy data served to produce seasonal CO₂ flux maps. In 2002, the mid-latitude North Atlantic was a year-round sink and took up 1.9 mol m⁻² yr⁻¹.

1. Introduction

Volunteer observing ships (VOS) such as research and commercial vessels provide a large number of observations and ground truth for satellite data. Recently in the North Atlantic Ocean, efforts have been made to outfit more VOS with automated sensors to measure the partial pressure of CO₂ in surface water. A larger database of surface ocean carbon data is, therefore, now available. However, the production of regional CO₂ flux maps from ocean CO₂ observations alone is limited by the spatial and temporal extent of the individual cruises. Empirical relationships between the sea surface fugacity of CO₂ (fCO_{2 sw}) and a number of remote sensing and field data can be used to create high resolution regional flux maps which extend the coverage provided by ship observations alone (e.g., Olsen *et al.*, 2004; Lefèvre *et al.*, 2004; Nelson *et al.*, 2001).

Different mechanisms affect the carbon cycle in the Atlantic Ocean north of 30°N. The fCO_{2 sw} is changed by thermodynamics, biology, mixing, and air-sea gas exchange. The thermodynamic relationship between seawater fCO_{2 sw} and temperature is well known (Takahashi *et al.*, 1993; Weiss *et al.*, 1982), whereas the effects of biological production and mixing are more difficult to resolve. Photosynthesis and respiration change the carbon concentration and thus affect the fCO_{2 sw}. Chlorophyll is a measure of algal biomass and can be derived from optical satellite data, but its use as a fCO_{2 sw} proxy has been rather limited (e.g., Watson *et al.*, 1991; Ono *et al.*, 2004). A parameter of fundamental importance for changes in the upper water column is the MLD, and it is a promising tool for the prediction of surface fCO_{2 sw}. A deep mixed layer usually brings up nutrient-rich waters with high concentrations of dissolved inorganic carbon (DIC). This process will increase the fCO_{2 sw} in the upper layer while, on the other hand, a strong stratification will prevent this transport. MLD climatologies are

available, but they do not reflect the interannual changes. As an alternative, MLD data on a regional scale can be obtained from profiling float temperature data such as provided by the Argo project. More than 3000 floats have been deployed to date in the global oceans. These profilers automatically record temperature and salinity on ten-day intervals between the surface ocean and a depth of 2000 m (<http://www.aoml.noaa.gov/phod/argo/index.php>).

In this work, data from two container ships, one car carrier, and two research vessels are combined and co-located with SST data from satellite observations and mixed layer depths from Argo data. This dataset is then used to create $f\text{CO}_{2\text{sw}}$ algorithms for different biogeochemical provinces which are loosely based on the definitions by Longhurst (1995). The algorithms are subsequently applied to satellite and Argo data on a $2^\circ \times 2^\circ$ resolution. Seasonal flux maps are created, and the annual CO_2 uptake is presented for each province. The high resolution CO_2 fluxes are also compared to fluxes calculated by using a simple interpolation method and the climatology of Takahashi *et al.* (2002).

2. Hydrographic Setting

The North Atlantic can be subdivided into a subtropical and a subpolar domain. The main surface currents in the subtropical region are the Gulf Stream and the North Atlantic Current. The Gulf Stream is defined as the northward-flowing current from the Straits of Florida to the Newfoundland Basin. This current carries water of higher salinity and 18°C is usually considered as the lower SST limit (Longhurst, 1995). The North Atlantic Current flows northeastward, and part of it covers a strong temperature gradient which is denoted as the Subarctic Front. This is located between the Flemish Cap and the Mid-Atlantic Ridge around 52°N (Krauss, 1986). This region typically displays a deep winter mixed layer of up to 500 m. In spring, phytoplankton blooms migrate northward along the North Atlantic Current with chlorophyll values of about 0.2 $\mu\text{g/L}$ at the onset of the bloom.

The subpolar region is characterized by various surface currents. The Labrador Current originates in the Labrador Sea, flows southward, and eventually feeds into the North Atlantic Current. The East Greenland Current originates in the Arctic Ocean and flows south along the East Greenland coast. At Cape Farewell, it meets with the Irminger Current and flows southwestwardly around Greenland into the Labrador Sea and forms, on its subsequent northward flow, the West Greenland Current. The onset of spring blooms typically occurs earlier here than at lower latitudes (Tomczak and Godfrey, 2003).

The VOS observations are separated into geographical regions similar to the biogeochemical provinces defined by Longhurst (1995): the North Atlantic Drift (NADR); the Atlantic Arctic gyre (ARCT); and the Gulf Stream (GFST). The Longhurst provinces are used as guidelines, and the boundaries and biogeochemical characteristics deviate from the original description depending on cruise coverage (Figure 1). Hydrographic details for each regime are presented in section 4.

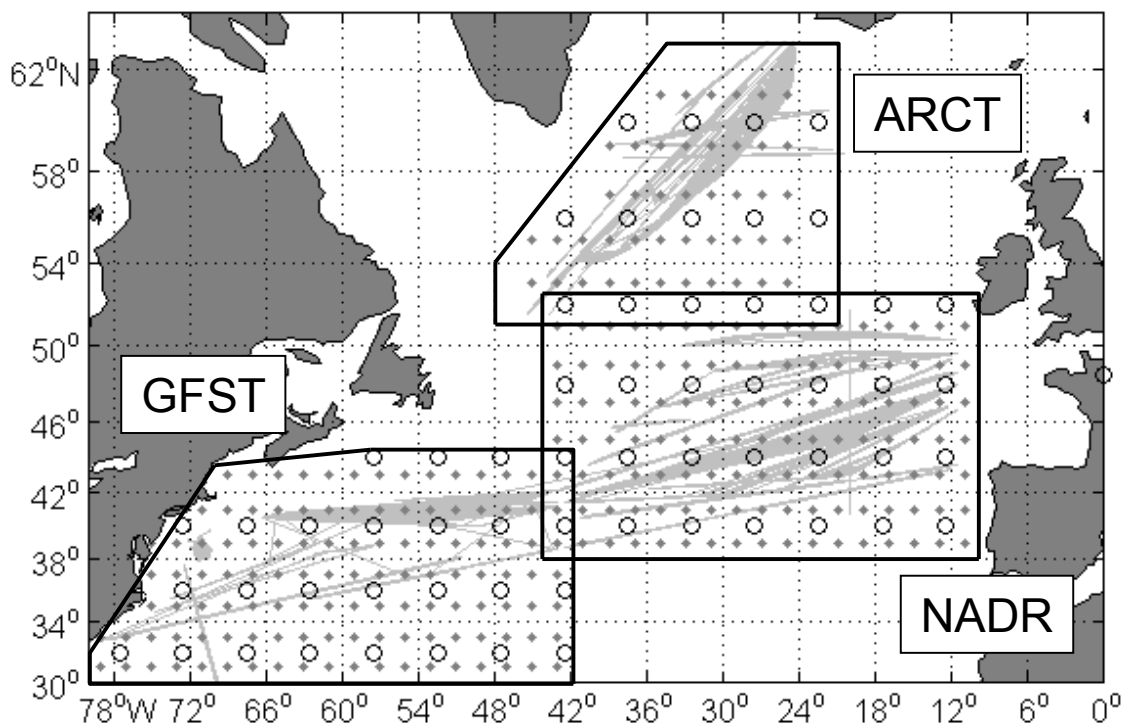


Figure 1: VOS cruises (gray lines) and boundaries of the three provinces that were used in the analysis. The gray circles denote the $2^\circ \times 2^\circ$ grids, while the open white circles display the Takahashi *et al.* (2002) grid ($4^\circ \times 5^\circ$). ARCT: Atlantic Arctic province; NADR: North Atlantic Drift; GFST: Gulf Stream. The overlapping $2^\circ \times 2^\circ$ grids between the NADR and GFST provinces were compared and yielded nearly identical flux results (not shown).

3. Data and Methods

3.1. $f\text{CO}_2_{\text{sw}}$ Data

The VOS data used in this work were obtained from the following commercial and research vessels: M/V *Falstaff*; M/V *Nuka Arctica*; M/V *Skogafoss*; R/V *Ronald H. Brown*; and the R/V *Meteor*. The M/V *Falstaff* is a car carrier that sails in the North Atlantic, usually between Southampton, United Kingdom, and New York, United States (Table 1). Data were collected on 16 trips between February 2002 and May 2003. The container ship M/V *Nuka Arctica* runs between Greenland and Denmark, and data from three of its round trips from 2004 were included. The M/V *Skogafoss*, a container ship, operates between Boston, Massachusetts and Reykjavik, Iceland. Data from its cruises in 2004 and 2005 were used. The U.S. research vessel R/V *Ronald H. Brown* covered this region in 2002, and the German research vessel R/V *Meteor* sailed in this region in spring 2004.

The $f\text{CO}_2_{\text{sw}}$ instruments on the ships were all based on the same principles. Onboard the M/V *Falstaff*, a Japanese system was installed that is described in more detail in Lueger *et al.* (2004). The systems onboard the M/V *Nuka Arctica* and the M/V *Skogafoss* are commonly referred to as Neill systems after the designer and builder Craig Neill. The measurement system onboard the R/V *Ronald H. Brown* is based on the system described in Feely *et al.* (1998), whereas the $f\text{CO}_2_{\text{sw}}$ system that was used on the M60 cruise onboard the R/V *Meteor* is described in Körtzinger (1999).

Table 1. Cruises on Volunteer Observing Ships that were used in this work. The validation cruises are not shown.

Province	Ship	Cruise	Year	Starting Month	N
NADR	<i>Falstaff</i>	Fal-01	2002	2	1042
NADR	<i>Falstaff</i>	Fal-03	2002	4	212
NADR	<i>Falstaff</i>	Fal-04	2002	5	213
NADR	<i>Falstaff</i>	Fal-05	2002	5	943
NADR	<i>Falstaff</i>	Fal-06	2002	6	759
NADR	<i>Falstaff</i>	Fal-07	2002	7	1341
NADR	<i>Falstaff</i>	Fal-08	2002	7	273
NADR	<i>Falstaff</i>	Fal-09	2002	8	790
NADR	<i>Falstaff</i>	Fal-11	2002	9	842
NADR	<i>Falstaff</i>	Fal-12	2002	10	1362
NADR	<i>Falstaff</i>	Fal-13	2002	11	1099
NADR	<i>Falstaff</i>	Fal-15	2002	12	369
NADR	<i>Falstaff</i>	Fal-16	2003	1	1271
NADR	<i>Falstaff</i>	Fal-17	2003	2	1625
NADR	<i>Falstaff</i>	Fal-19	2003	5	223
NADR	<i>Ronald H. Brown</i>	304B	2003	6	632
				sum	12996
ARCT	<i>Skogafoss</i>	402	2004	2	154
ARCT	<i>Skogafoss</i>	409	2004	5	348
ARCT	<i>Skogafoss</i>	408_1	2004	5	76
ARCT	<i>Skogafoss</i>	411	2004	7	108
ARCT	<i>Skogafoss</i>	414	2004	10	188
ARCT	<i>Skogafoss</i>	415	2004	11	250
ARCT	<i>Skogafoss</i>	416	2004	12	683
ARCT	<i>Skogafoss</i>	502	2005	2	129
ARCT	<i>Skogafoss</i>	503	2005	3	414
ARCT	<i>Nuka Arctica</i>	150304	2004	3	237
ARCT	<i>Nuka Arctica</i>	240204	2004	2	165
ARCT	<i>Nuka Arctica</i>	310804	2004	9	349
				sum	3101
GFST	<i>Falstaff</i>	Fal-01	2002	3	196
GFST	<i>Falstaff</i>	Fal-02	2002	3	84
GFST	<i>Falstaff</i>	Fal-03	2002	4	369
GFST	<i>Falstaff</i>	Fal-05	2002	5	697
GFST	<i>Falstaff</i>	Fal-06	2002	6	82
GFST	<i>Falstaff</i>	Fal-07	2002	7	987
GFST	<i>Falstaff</i>	Fal-08	2002	7	836
GFST	<i>Falstaff</i>	Fal-09	2002	8	675
GFST	<i>Falstaff</i>	Fal-12	2002	10	524
GFST	<i>Falstaff</i>	Fal-13	2002	11	921
GFST	<i>Falstaff</i>	Fal-14	2002	11	573
GFST	<i>Falstaff</i>	Fal-16	2003	1	114
GFST	<i>Falstaff</i>	Fal-19	2003	5	66
GFST	<i>Ronald H. Brown</i>	207	2002	9	803
GFST	<i>Ronald H. Brown</i>	208T	2002	9	760
GFST	<i>Skogafoss</i>	409	2004	6	10
				sum	7697

All systems show a broad commonality. Seawater is pumped from the intake of the ship at a varying rate into the thermosalinograph and equilibrator. In the equilibrator, the water is equilibrated with headspace air, and a sample of this air is pumped into the measurement unit. All systems use a non-dispersive infrared analyzer (NDIR-LiCOR[®]), which is controlled by external software. The air sample is dried in several steps, usually including a condenser, Permapure Nafion[®] drier and a chemical drying agent, and magnesium perchlorate before it enters the NDIR unit where the CO₂ concentration is analyzed and recorded as the mole fraction (xCO₂).

The CO₂ fugacity, which accounts for the non-ideal behavior of CO₂, was computed from the calibrated xCO₂ according to equation 1 (DOE, 1994). The nominal difference between partial pressure of CO₂ (pCO_{2 sw}) and the fugacity (fCO_{2 sw}) is 0.3% (≈0.1 μatm), with fCO_{2 sw} being lower.

$$fCO_{2\ eq} = xCO_2 \cdot (p - p_{H_2O}) \cdot \exp\left(p \cdot \frac{(B + 2\delta)}{RT_{eq}}\right) \quad (1)$$

where p is the equilibrator pressure (atm), p_{H₂O} is the saturation water vapor pressure (atm), B is the first virial coefficient of CO₂, δ is the cross virial coefficient, R is the ideal gas constant (82.0578 cm³ atm mol⁻¹ K⁻¹), and T_{eq} is the equilibrator temperature in K. The water vapor pressure, p_{H₂O} (atm), is given by Weiss and Price (1980):

$$p_{H_2O} = \exp\left(24.4543 - 67.4509 \cdot \left(\frac{100}{T_{eq}}\right) - 4.8489 \cdot \ln\left(\frac{T_{eq}}{100}\right) - 0.000544 \cdot S\right) \quad (2)$$

where S is the sea surface salinity.

The first virial coefficient, B (cm³ mol⁻¹), and the cross virial coefficient, δ (cm³ mol⁻¹), are calculated according to Weiss (1974) using the equilibrator temperature:

$$B = -1636.75 + 12.0408 \cdot T_{eq} - 3.27957 \cdot 10^{-2} \cdot T_{eq}^2 + 3.16528 \cdot 10^{-5} \cdot T_{eq}^3 \quad (3)$$

$$\delta = 57.7 - 0.118 \cdot T_{eq} \quad (4)$$

The fCO_{2 eq} value needs to be corrected to account for any bias introduced by the difference between the equilibrator (T_{eq}) and the in situ (T_{is}) temperature. The following correction scheme by Takahashi *et al.* (1993) was applied which results in the in situ fCO_{2 sw}:

$$fCO_{sw} = fCO_{2\ eq} \cdot \exp(0.0423 \cdot (T_{is} - T_{eq})) \quad (5)$$

3.2. Satellite and Argo Data

The AVHRR SST data were obtained from the Physical Oceanography Distributed Active Archive Center (PODAAC) at NASA's Jet Propulsion Laboratory in Pasadena, California (<http://poet.jpl.nasa.gov/>), and they were co-located with the original $f\text{CO}_2_{\text{sw}}$ data retrieved from the shipboard data. The AVHRR data has a nominal spatial resolution of 9 km and an accuracy of 0.5-0.7°C. The co-location criteria, or cut-off limits, for the satellite observations are 25 km and 12 hours. The AVHRR data were screened for cloud contamination using the NAVOCEANO algorithm which discriminates clouds and extracts the SST from the AVHRR data using a non-linear relationship (Walton *et al.*, 1998). The agreement of the AVHRR SST data with the SST data measured onboard the VOS is shown in Figure 2. The mean deviation between measured SST and satellite data is $0.2 \pm 0.53^\circ\text{C}$ with the satellite data being lower possibly due to the thermal skin effect (Robertson and Watson, 1992). The bias is constant within the co-location limits, and no trend is observed by cruise or ship.

The global Argo data were provided by the U.S. Argo Center (<http://www.aoml.noaa.gov/phod/ARGO/HomePage/>). Mixed layer depth was computed from the individual temperature profiles as the depth at which a 0.1°C difference from a near surface value occurs. The MLD data from 2002-2005 were gridded to yield monthly mean values at a resolution of 2° latitude and 4° longitude (courtesy H. Yang and R. Molinari, NOAA/AOML).

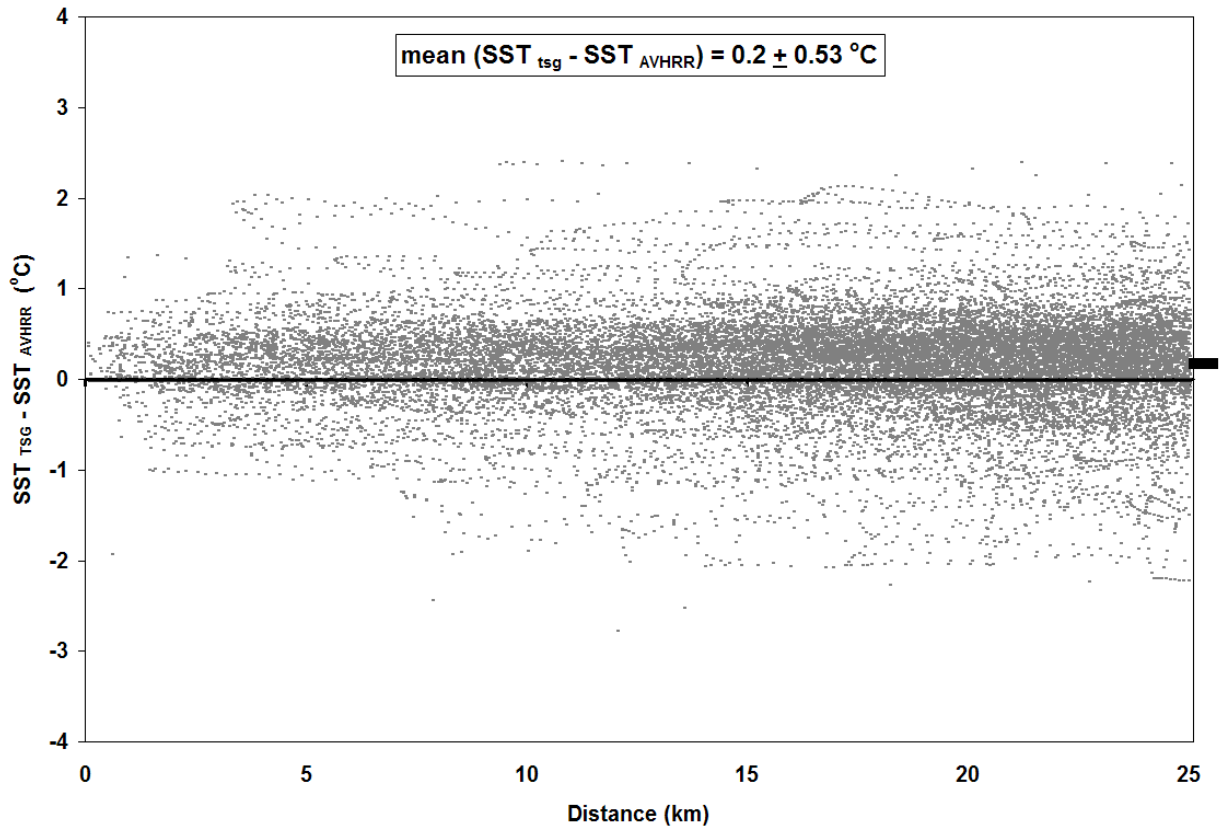


Figure 2: Difference between SST observed onboard the VOS (SST_{TSG}) and SST retrieved from AVHRR (SST_{AVHRR}) versus the distance between the satellite and ship data ($n = 24,382$).

The level 2B wind speed product retrieved from NASA's Quick Scatterometer, QuikSCAT, has a resolution of 25 km and was used for the flux calculations. The data are available from PODAAC at <http://podaac.jpl.nasa.gov>. Wind speed products from individual retrievals were employed to coincide with the various approaches that are described in more detail in sections 3.3-3.5 and Table 2.

The $fCO_{2\text{sw}}$ algorithms were developed in a step-by-step procedure. At first, all VOS data were gathered in an effort to relate $fCO_{2\text{sw}}$ to relevant parameters such as SST, chlorophyll, and MLD which resulted in poor fits with high RMS values. To minimize the RMS values, the VOS data were subdivided into provinces. For each province, simple linear regressions between $fCO_{2\text{sw}}$ and SST, chlorophyll, or MLD were tested which still yielded very poor fits. The next step used multi-linear approaches which combined SST and MLD data in a single regression. Since the RMS values were still too high, a polynomial regression method was employed which considerably improved the fits. Seasonal algorithms were also tested and so were algorithms including chlorophyll data; these approaches are described in section 3.6, and they yielded no satisfactory results.

The algorithms were calculated with the computer program SigmaPlot[®] which uses the Marquardt-Levenberg routine to estimate the non-linear parameters based on the least squares method (Press *et al.*, 1986). For all provinces except NADR, the observed seawater $fCO_{2\text{sw}}$, AVHRR SST, and MLD data were taken as is in order to determine the optimal algorithm. The $fCO_{2\text{sw}}$ data used in the NADR algorithm had more uncertainty associated with them, and outliers were removed by excluding data above and below a limit of 2 sigma (standard deviation).

Table 2: Data sources used to compute the CO₂ flux for the three approaches. The climatology by Takahashi *et al.* (2002) for the virtual year 1995 is normalized to 2002.

Dataset	Algorithm (F _{2x2})	Cruise Avg (F _{4x5})	Takahashi et al. (F _{4x5} climato)
Resolution	2°x2°/monthly	4°x5°/monthly	4°x5°/monthly
Flux year	2002	2002	2002
Seawater $fCO_{2\text{sw}}$	Algorithm MLD: Argo (2°x2°/monthly) SST: AVHRR (2°x2°/monthly)	Cruise averages	Climatology NADR/GFST: 1995 ARCT: 1995
Atmospheric fCO_2	Monthly flask data (2002)	Monthly flask data (2002)	NADR/GFST: 1995 ARCT: 2002
Wind speed	QuikSCAT (2°x2°/monthly) 2002	QuikSCAT (4°x5°/monthly) 2002	QuikSCAT (4°x5°/monthly) 2002
SST	AVHRR (2°x2°/monthly) 2002	Cruise averages	Climatology (1995)

3.3. CO₂ Flux Calculation based on Algorithms (F_{2x2})

CO₂ fluxes on a 2° × 2° resolution (F_{2x2} = proxy fluxes) were calculated using various fCO_{2 sw} algorithm data (fCO_{2 sw/2x2}) that are described in section 4. Table 2 lists the data sources and years of collection for the different flux calculations. The flux was calculated according to:

$$F = (f\text{CO}_2_{\text{sw}/2x2} - f\text{CO}_2_{\text{atm}}) k K_0 = \Delta f\text{CO}_2 k K_0 \quad (6)$$

The fCO₂ gradient across the air-sea interface is commonly referred to as the ΔfCO₂ and is the difference between seawater and atmospheric fCO₂. The fCO_{2 sw/2x2} data were calculated from the province-specific algorithms. The atmospheric fCO₂ values for 2002 were calculated from monthly xCO₂ averages. The average monthly values taken from four stations of NOAA's Earth System Research Laboratory (Global Monitoring Division, formerly the Climate Monitoring and Diagnostics Laboratory) network around the North Atlantic Ocean—Mace Head, Ireland (MHD), Azores, Portugal (AZR), Bermuda (BME), and Iceland (ICE)—were used (Tans and Conway, 2005). The atmospheric mole fractions were converted into fCO₂ by using equation 1 and replacing T_{eq} by SST data. Employing equations 1-4, SST is from AVHRR, and sea level pressure (SLP) data are from the NCEP/NCAR (National Centers for Environmental Prediction/National Center for Atmospheric Research) reanalysis project (Kalnay *et al.*, 1996). Both SST and SLP data are monthly values with a 2° × 2° resolution. Most of the VOS observations were taken in 2002 and, therefore, the flux results represent this year. However, in the ARCT province data from the year 2004 were used the most. In this case, the seawater fCO_{2 sw/2x2} data were calculated by using AVHRR SST from 2004, whereas Argo MLD (2002-2005) were the same as for the NADR and GFST provinces. The atmospheric fCO₂ data of the ARCT were retrieved from the 2004 flask data. For the analysis over the entire region, it was assumed that the ΔfCO₂ did not change over the two-year period.

The solubility, K₀ (Weiss, 1974), was calculated using 2° × 2° AVHRR SST and assuming a salinity of 35. The transfer velocity, k, was computed on a 2° × 2° resolution using individual QuikSCAT wind speed retrievals from 2002:

$$k_{\text{av}} = 0.31 U_{\text{av}}^2 \left((\Sigma U^2 / n) / (U_{\text{av}})^2 \right) (\text{Sc} / 600)^{-1/2} = (0.31 \Sigma U^2 / n) (\text{Sc} / 660)^{-1/2} \quad (7)$$

where (ΣU²/n) is the second moment, U_{av} is the monthly mean, and ((ΣU²/n)/(U_{av})²) is also referred to as the non-linearity factor, R. This factor was included to retrieve a better statistical representation of the wind speed and is described in detail in Wanninkhof *et al.* (2002). The second moment represents the variance of the wind speed, and n is the number of observations (between 2300 and 3400 per month and a 2° × 2° grid cell). Sc is the Schmidt number and was calculated according to Wanninkhof (1992) using monthly gridded AVHRR SST fields (monthly value of the 2° × 2° grid). In all provinces, monthly F_{2x2} data representing 2002 were averaged to seasonal fluxes, i.e., three-monthly averages, to create the maps in Figures 8 and 9.

3.4. CO₂ Flux Calculation based on Cruises (F_{4x5})

The F_{4x5} estimates for each province for 2002 were calculated using equations 6 and 7, and they were based on a monthly 4° × 5° resolution. The ΔfCO₂ and SST data were retrieved by bin averaging the original cruise data. The atmospheric fCO₂ values were calculated from

monthly ESRL $x\text{CO}_2$ averages. The transfer velocity, k , was calculated using 2002 QuikSCAT wind speed data with $4^\circ \times 5^\circ$ resolution (see equation 7 and Table 2).

3.5. CO_2 Flux Calculation based on Climatology ($F_{4 \times 5 \text{ climatol}}$)

The atmospheric and seawater CO_2 partial pressures provided by Takahashi *et al.* (http://www.ldeo.columbia.edu/res/pi/CO2/carbondioxide/air_sea_flux/pco2_940.txt) were converted into $f\text{CO}_{2 \text{ climat}}$ by using equations 1-4. The SST and SLP data provided with the climatological $p\text{CO}_2$ data were used for this purpose. The flux was calculated using equation 6 with the k values determined as in section 3.4 using climatological SST.

The Takahashi *et al.* (2002) climatology was projected onto the year 1995 assuming that the parallel increase of atmospheric and seawater $f\text{CO}_2$ due to the rising atmospheric CO_2 concentration did not apply to regions north of 45°N . It was assumed that the $f\text{CO}_{2 \text{ sw}}$ remains invariant over time due to deep convective mixing. This assumption was followed in the present work, and for the northernmost province (ARCT) only the atmospheric $f\text{CO}_2$ ($f\text{CO}_{2 \text{ atm/climat}}$) values were corrected for the temporal increase in $f\text{CO}_2$ by adding ($7 \cdot 1.6 =$) $11.6 \mu\text{atm}$. The climatological seawater $f\text{CO}_2$ ($f\text{CO}_{2 \text{ sw/climat}}$) values were left unchanged, thus leading to an increasing $\Delta f\text{CO}_{2 \text{ climat}}$ over time. In the case of the NADR and GFST provinces, the $\Delta f\text{CO}_{2 \text{ climat}}$ data were taken as is since Takahashi *et al.* (2002) assumed that the sea surface $p\text{CO}_2$ in these regions increased at the same rate as the atmospheric $p\text{CO}_2$.

3.6. Satellite Chlorophyll Data

Since the $f\text{CO}_{2 \text{ sw}}$ of the surface ocean is to a large extent controlled by biology, it is worthwhile to discuss why $f\text{CO}_{2 \text{ sw}}$ did not correlate well with satellite chlorophyll data. Chlorophyll is a biological parameter that reflects ocean production. In the spring, sunlight availability steadily increases, and the mixed layer containing nutrients, entrained during the winter, rapidly warms and becomes shallow. This setting stimulates productivity and algae growth which is reflected in enhanced chlorophyll concentration. As a result of higher production, the surface seawater, $f\text{CO}_2$, decreases since the phytoplankton takes up CO_2 for the process of photosynthesis. One would expect a close and inverse relationship between chlorophyll and $f\text{CO}_{2 \text{ sw}}$, especially during spring season, but it is likely that prediction is restricted to the spring at best. The reason is that a decrease in chlorophyll, after the decay of an algal bloom, will not correlate directly with an increase in $f\text{CO}_{2 \text{ sw}}$. Both DIC and $f\text{CO}_{2 \text{ sw}}$ will take more time to be restored to original concentration by means of upwelling, mixing, or air-sea gas exchange.

In this dataset, the underway data were co-located with SeaWiFS (Sea-viewing Wide Field of View Sensor) and MODIS (Moderate Resolution Imaging Spectroradiometer) chlorophyll data, and several approaches were tested to find a reliable algorithm. A similar concept was also tested in an earlier publication where temperature normalized $p\text{CO}_{2 \text{ sw}}$ was compared with observed and SeaWiFS chlorophyll, and no significant correlation could be established, either in time and/or space (Lueger *et al.*, 2004).

In the present work, no meaningful correlation for any temporal and/or spatial resolution could be found that was more accurate than the algorithms using satellite temperature and Argo mixed layer depth data alone. In all cases (e.g., seasonal, annual, provinces, entire region), the addition of chlorophyll did not enhance the performance of the algorithms, nor did the single use of chlorophyll within an algorithm, e.g., when using chlorophyll and position information alone. Additionally, it was tested if the use of temperature-normalized $f\text{CO}_{2\text{sw}}$ would yield satisfactory results when combined with satellite chlorophyll, but no useful algorithms were found.

The following gives an example of this finding and, since the correlation is expected to be strong in late spring, this season serves as a case study. Table 3 compares the statistics for the spring algorithms that resulted when chlorophyll data were included or excluded in the algorithms. In all three provinces, the additional use of chlorophyll information in the algorithm did not significantly improve the algorithm.

Using chlorophyll data from satellite observations for $f\text{CO}_{2\text{sw}}$ prediction is furthermore hampered by the fact that there are far less data available than, for example, AVHRR temperature. In the case of the MODIS satellite chlorophyll data, approximately two passes per day covered the regions whereas, in the case of AVHRR SST, five to six daily passes were reported. This explains the much lower data yield when including chlorophyll data. The example suggests that, at least for this dataset, even during the spring satellite observations including ocean color do not yield any better estimates of surface $f\text{CO}_{2\text{sw}}$ than compared with just using SST and MLD.

Table 3: Comparison of the statistical results in the spring (April-June) for predicted $f\text{CO}_{2\text{sw}}$ data within the three provinces (NADR, ARCT, GFST) retrieved by regression analysis. Predictors are AVHRR SST, Argo mixed layer depth, and position including and excluding MODIS chlorophyll within the algorithm. RMS: root mean square error (random error); r^2 : regression coefficient; mean residual difference: average of the residuals (=bias); data points: number of data points used for algorithm.

Province	Months	RMS (Random Error) Algorithm	r^2 Algorithm	Mean Residual Difference Algorithm	Data Points Algorithm	Data Sources Algorithm
NADR	Apr/May/June	9.91	0.49	0.00	1694	AVHRR SST/Argo MLD
		9.91	0.49	0.00	1694	AVHRR SST/Argo MLD + MODIS CHL
ARCT	Apr/May/June	5.37	0.85	-0.01	252	AVHRR SST/Argo MLD
		5.13	0.86	0.00	252	AVHRR SST/Argo MLD + MODIS CHL
GFST	Apr/May/June	5.76	0.61	-0.07	532	AVHRR SST/Argo MLD
		5.75	0.62	-0.10	532	AVHRR SST/Argo MLD + MODIS CHL

4. Algorithms

4.1. North Atlantic Drift Province (NADR)

The NADR province is characterized by the North Atlantic Current, which flows northeastwardly from approximately 40°N (Longhurst, 1995). To the south, this province is demarked by the southeastward drift of the Azores Current at about 45°N (Krauss, 1986).

To attain an algorithm with the highest possible accuracy, the VOS data within the NADR province were tested using different input parameters. A strong correlation between seawater $f\text{CO}_{2\text{sw}}$ and AVHRR SST was expected which, however, yielded an RMS of over 13 μatm when employing a third-order polynomial relationship between $f\text{CO}_{2\text{sw}}$ and SST. Position and mixed layer depth data were added to the variables and this improved the overall accuracy. The addition of satellite chlorophyll data was not successful, as discussed earlier in section 3.6.

The final NADR algorithm was created with observations from the M/V *Falstaff* and R/V *Ronald H. Brown*, and it covered the region between 39°-51°N and 11°-43°W (Table 1). The measured sea surface salinity (SSS) and SST data ranged from 32.79-36.85, and from 10°-25.5°C, respectively. The measured seawater $f\text{CO}_{2\text{sw}}$ reveals maximum and minimum values of 402 and 282 μatm , respectively. A third-order polynomial between seawater $f\text{CO}_{2\text{sw}}$ and AVHRR-SST and a first-order relationship between $f\text{CO}_{2\text{sw}}$ and Argo mixed layer depth yielded the smallest RMS:

$$\begin{aligned} f\text{CO}_{2\text{sw}} = & 7.1 \cdot (\pm 2.3) \text{ SST} - 1.4 \cdot (\pm 0.1) \text{ SST}^2 + 0.05 \cdot (\pm 0.0) \text{ SST}^3 \\ & + 0.2 \cdot (\pm 0.0) \text{ MLD} + 0.4 \cdot (\pm 0.0) \text{ LON} - 1.2 \cdot (\pm 0.0) \text{ LAT} + 435.4 (\pm 12.5) \\ n = & 12,996, \quad r^2 = 0.62, \quad \text{RMS} = 9.75 \mu\text{atm}. \end{aligned} \quad (8)$$

The numbers in parenthesis are the error values of the coefficients. Longitude is expressed as degree West. Since monthly averages for MLD data were used, the error range is close to zero. The cruises in this province were along very similar tracks, and this led to the small error values for the position coefficients. The maximum and minimum residuals, when comparing the measured and predicted $f\text{CO}_{2\text{sw}}$, are +41 and -28 μatm , respectively. A summary is given in Table 4, and the residuals are compared with the predicted $f\text{CO}_{2\text{sw}}$ in Figure 3.

The algorithm was validated with data from the M/V *Falstaff* that were not included when retrieving the algorithm. These data were randomly excluded, and a total of 687 data points yielded a similar RMS (11.4 μatm) and a r^2 value of 0.69. The maximum and minimum deviations were calculated at 19 and -31 μatm , respectively. As a test, these data points were also included in the original dataset, and the resulting algorithm was similar to equation 8, which assures that both the validation and the algorithm data show a very similar pattern between $f\text{CO}_{2\text{sw}}$ and AVHRR temperature and Argo mixed layer depth.

Table 4: Statistical results for predicted $fCO_{2\text{sw}}$ data within three provinces (NADR, ARCT, GFST) retrieved by regression analysis. Predictors are AVHRR SST and Argo mixed layer depth. RMS: root mean square error (random error); r^2 : regression coefficient; mean residual difference: average of the residuals (=bias); data points: number of data used for algorithm; validation: independent data used to test the algorithms.

Province	Months	Years	RMS (Random Error) Algorithm	r^2 Algorithm	Mean Residual Difference Algorithm	Data Points Algorithm	Data Sources Algorithm
NADR	Jan-Dec	2002/2003	9.75	0.62	-0.13	12996	AVHRR SST/Argo MLD
ARCT	Jan-Dec*	2004/2005	10.37	0.77	0.00	3101	AVHRR SST/Argo MLD
GFST	Jan-Dec	2002/2004	9.47	0.79	-0.12	7697	AVHRR SST/Argo MLD

Province	Months	Years	RMS (Random Error) Validation	r^2 Validation	Mean Residual Difference Validation	Data Points Validation	Data Sources Validation
NADR	Feb/May-Aug/Oct/Nov	2002/2003	11.44	0.69	-3.97	687	AVHRR SST/Argo MLD
ARCT	Feb/Mar/Jun	2004	10.32	0.81	-7.39	234	AVHRR SST/Argo MLD
GFST	Mar/May/Jun/Sep	2002/2004	9.97	0.87	-7.56	552	AVHRR SST/Argo MLD

*No data available for April and August.

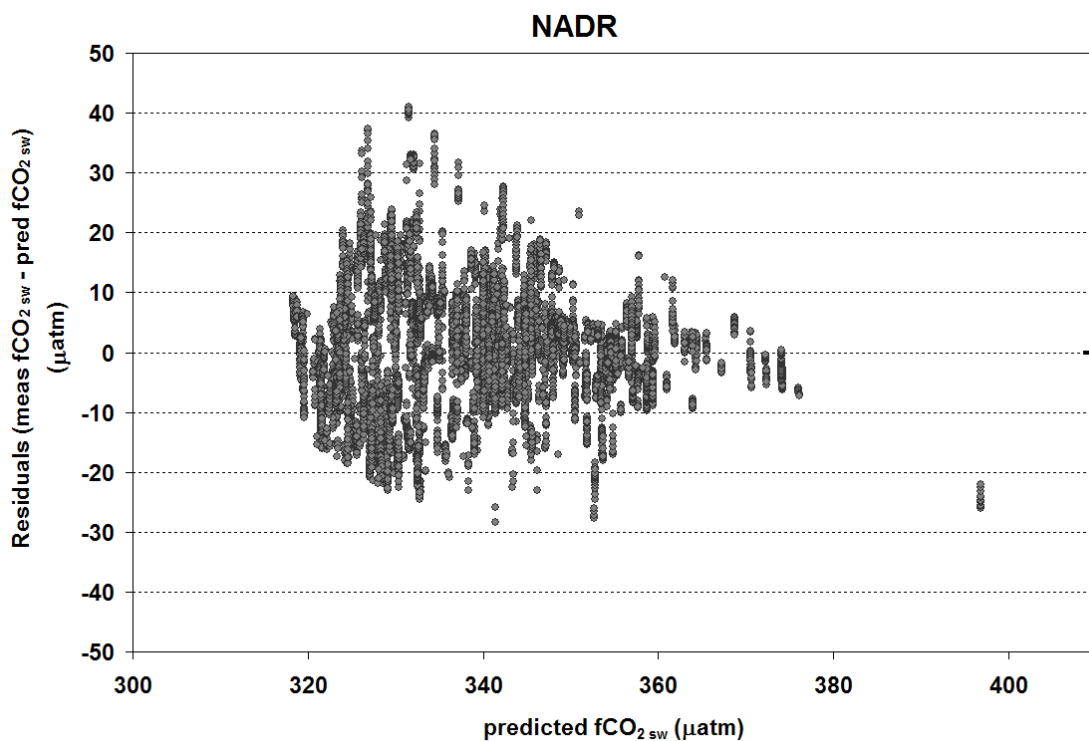


Figure 3: Comparison of the residuals and predicted $fCO_{2\text{sw}}$ data in the NADR province. The predicted $fCO_{2\text{sw}}$ data were retrieved from equation 8 by using temperature, mixed layer depth data (source: AVHRR/Argo), and position information. Also shown is the mean difference which is -0.1 μatm (black bar on the right).

4.2. Atlantic Arctic Province (ARCT)

The Atlantic Arctic (ARCT) province shows characteristics intermediate between Atlantic and Polar water. Its limits are the Polar Front to the south and the Greenland and Labrador coastal currents to the north and west. The data observed in this province were extremely variable and not clearly related to SST or SSS. Therefore, a sub-region was established based on SST and SSS signatures. This excluded low salinity data typically measured close to the coast. The ARCT province encompasses the region between 52°-63°N and 21°-46°W. It includes data measured onboard the M/V *Skogafoss* and M/V *Nuka Arctica*. SST and SSS ranged between 5.2°-13.3°C and 34.40-35.43, respectively. Many combinations were tested to achieve the highest accuracy and reliability for this algorithm including AVHRR SST, Argo MLD, and satellite chlorophyll in various approaches. In the ARCT province, as in the NADR, it was found that the addition of chlorophyll did not improve the algorithm (see section 3.6).

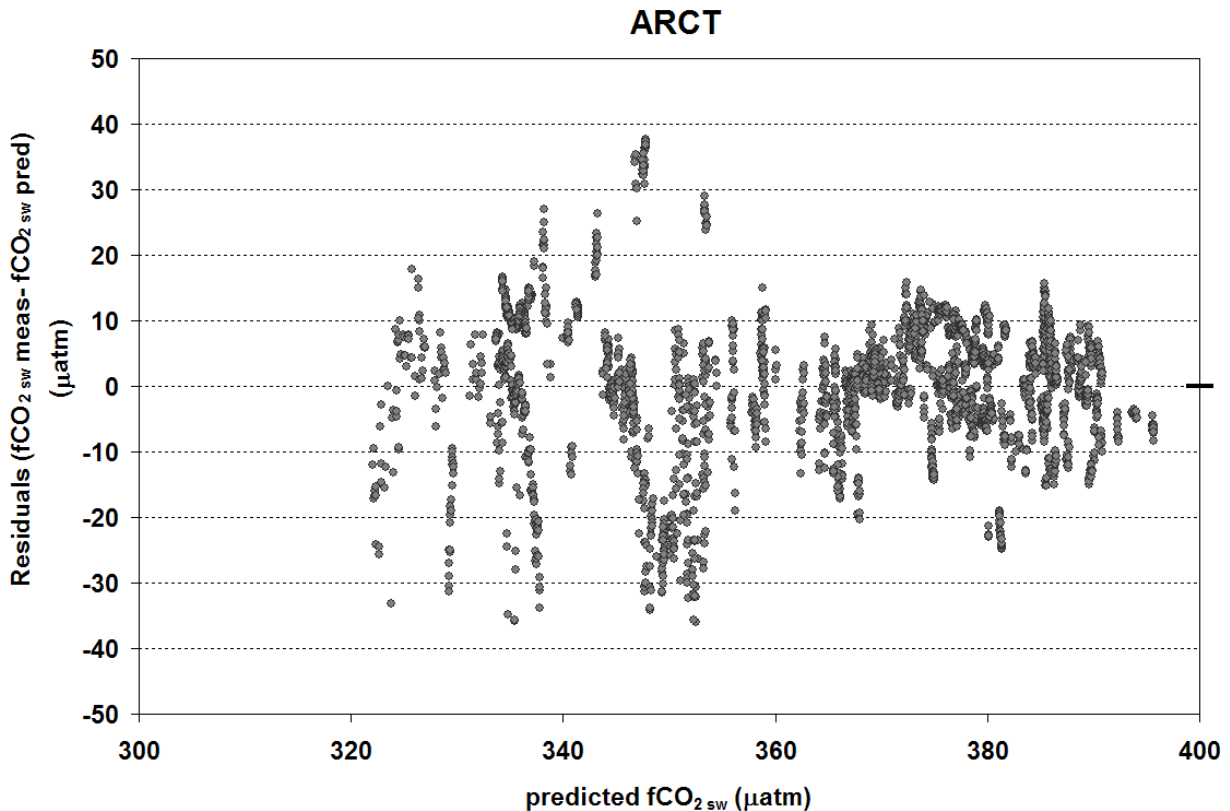


Figure 4: Comparison of the residuals and predicted $fCO_{2,sw}$ data in the ARCT province. The predicted $fCO_{2,sw}$ data were retrieved from equation 9 by using mixed layer depth data (source: Argo), SST (source: AVHRR), and position information. Also shown is the mean difference which is 0.00 μatm (black bar on the right).

The combination of AVHRR SST and Argo mixed layer depth yielded a relationship with the lowest RMS. An algorithm was created for $fCO_{2,sw}$ with a second-order dependency on SST and a first-order dependency on MLD. The direct comparison between measured and predicted $fCO_{2,sw}$ data is shown in Figure 4. The residuals range between 38 and -36 μatm . The algorithm for the ARCT province is:

$$\begin{aligned}
f\text{CO}_{2\text{ sw}} = & -14 \text{ SST } (\pm 0.9) + 0.7 \text{ SST}^2 (\pm 0.1) + 0.4 \text{ MLD } (\pm 0.0) \\
& + 0.6 \text{ LON } (\pm 0.1) + 0.5 \text{ LAT } (\pm 0.2) + 382 (\pm 12) \\
n = & 3101, \quad r^2 = 0.77, \quad \text{RMS} = 10.37 \mu\text{atm}.
\end{aligned} \tag{9}$$

Monthly averaged MLD data showed less variability than the other parameters in this algorithm. Compared with the NADR province, the cruise tracks in the ARCT province were more variable and, therefore, the errors are slightly higher compared with equation 8.

This algorithm was validated with cruises from the M/V *Nuka Arctica* and M/V *Skogafoss* that took place in February, March, and June 2004. The validation data yielded an RMS and a r^2 of 10.32 μatm and 0.81, respectively (Table 4). The minimal and maximal residuals were -44 and +13 μatm , respectively. The validation data had a bias (7.39 μatm). When including the validation data in the algorithm dataset, the algorithm was similar and the RMS value was identical.

4.3. Gulf Stream Province (GFST)

The GFST province considered here represents the northern extension of the Gulf Stream. The VOS data within this province were extracted from the original dataset based on SSS higher than 35 and yielded SSS and SST ranges from 35.0-37.4 and 4°-29°C, respectively. The spatial margins are from 19°-42°N and 43°-79°W, covering the northern extension of the subtropical gyre. These margins helped to refine the algorithm using SST and MLD. As with the ARCT and NADR provinces, satellite chlorophyll data had very little predictive power. The algorithm employed AVHRR SST, Argo mixed layer depth, and position information that covered the entire year. The residuals had maximal and minimal values of 36 and -40 μatm (Figure 5), respectively, and the algorithm is given by:

$$\begin{aligned}
f\text{CO}_{2\text{ sw}} = & -17.6 \text{ SST } (\pm 0.2) + 0.5 \text{ SST}^2 (\pm 0.0) - 1.4 \text{ MLD } (\pm 0.03) \\
& + 0.01 \text{ MLD}^2 (\pm 0.0) + 0.5 \text{ LON } (\pm 0.02) - 0.7 \text{ LAT } (\pm 0.03) + 578.3 (\pm 2.3) \\
n = & 7726, \quad r^2 = 0.79, \quad \text{RMS} = 9.47 \mu\text{atm}.
\end{aligned} \tag{10}$$

The validation data for this province were taken from observations onboard the R/V *Ronald H. Brown* and R/V *Meteor*, which cruised this region in 2002 and 2004. The RMS of 10.0 and the r^2 of 0.87 are similar to the algorithm (Table 4). The minimal and maximal residual was -34 and 35 μatm , respectively. As an additional test, we found that the inclusion of the validation data in the algorithm dataset resulted in a nearly identical equation and the bias was 7.56 μatm (Table 4).

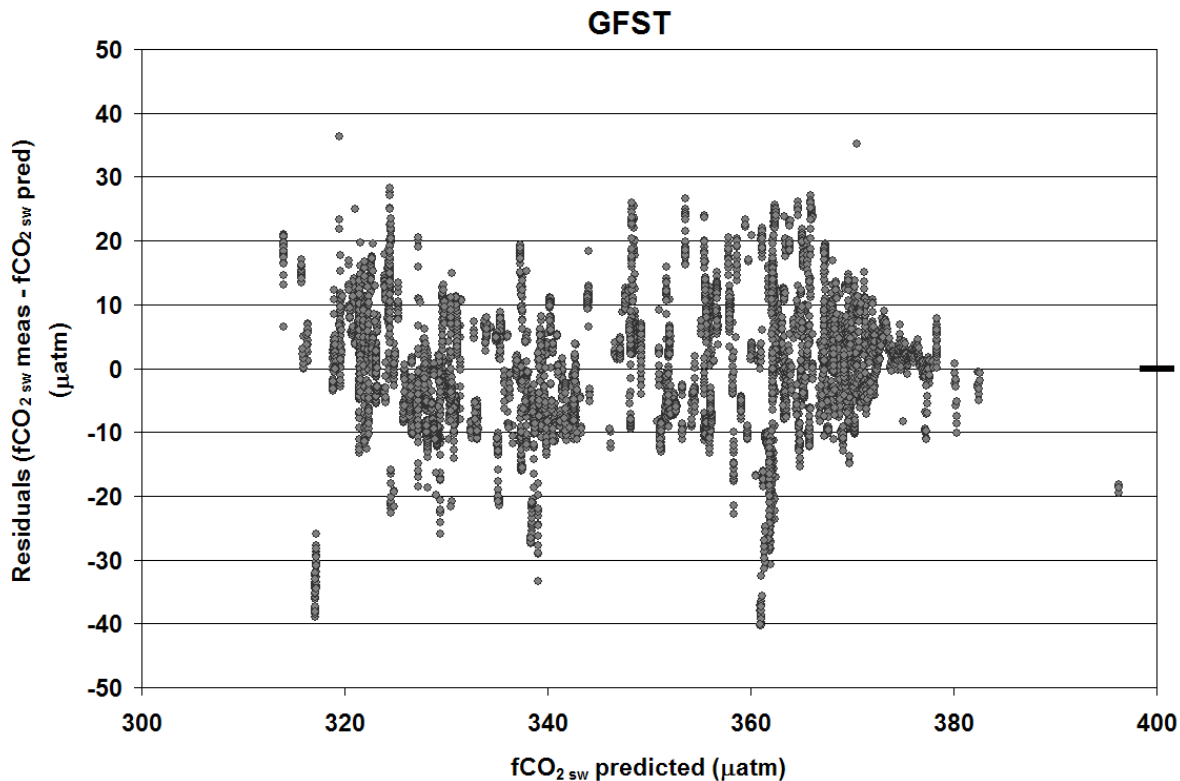


Figure 5: Comparison of the measured and the predicted $f\text{CO}_{2\text{sw}}$ data for the GFST province. The predicted $f\text{CO}_{2\text{sw}}$ data were retrieved by using equation 10 and AVHRR temperature, Argo mixed layer depth data, and position information for the algorithm data. Also shown is the mean difference which is $-0.12 \mu\text{atm}$ (black bar on the right).

5. Results and Discussion

5.1. Estimates of Seawater $f\text{CO}_{2\text{sw}}$

Sea surface $f\text{CO}_{2\text{sw}}$ proxy relationships strongly depend on the region. The good correlation between SST and $f\text{CO}_{2\text{sw}}$ is well known, and it has been repeatedly displayed especially in North Atlantic regions (Olsen *et al.*, 2004; Lefèvre *et al.*, 2004). Ono *et al.* (2004) used a combination of satellite SST and chlorophyll to extrapolate $p\text{CO}_2$ data in the North Pacific. In coastal regions such as river outlets, it has been shown that salinity is a good predictor of $f\text{CO}_{2\text{sw}}$ and can be used to estimate the CO_2 flux (Körtzinger, 2003).

The importance of the different mechanisms controlling surface $f\text{CO}_{2\text{sw}}$, such as the thermodynamic, biological, mixing, and air-sea gas exchange effects, varies among the three provinces. The thermodynamic $f\text{CO}_{2\text{sw}}$ steerer, SST, is empirically known to have an effect of $4.23\%/1^\circ\text{C}$ (Takahashi *et al.*, 1993), thus implying a positive correlation based on a simple linear regression. In the present study, we found varying patterns for the provinces. Based on linear regressions (not shown), the ARCT and NADR regions yield a negative $f\text{CO}_{2\text{sw}}$ -SST relationship while it is positive for the GFST. In the case of the ARCT and NADR provinces, the negative correlation between the two parameters can be explained as a result of upward transport of water masses with lower temperatures and higher respirational $f\text{CO}_{2\text{sw}}$ values. In the case of the GFST region, the $f\text{CO}_{2\text{sw}}$ -SST linear relationship yielded $1.56\%/1^\circ\text{C}$ based on the observed data. These

data are about one-third of the empirical value, indicating that other steerers are at play, such as, for example, mixing.

In the ARCT and NADR provinces, a positive correlation between MLD and $f\text{CO}_2_{\text{sw}}$ was found, whereas in the GFST the correlation was negative; again, this is based on a simple linear regression. This MLD- $f\text{CO}_2_{\text{sw}}$ pattern compares well with Lueger *et al.* (2004) where climatological MLD data were used. That work showed the MLD is negatively correlated to $p\text{CO}_2_{\text{sw}}$ in the western basin of the mid-latitude Atlantic, which compares with the GFST province, and positively in the eastern basin of the NADR. The GFST province, as part of the subtropical gyre, is a temperature-controlled regime where net community production is low compared with the more northerly provinces. The inverse relationship between MLD and $f\text{CO}_2_{\text{sw}}$ in the GFST may be explained by the following. When the MLD becomes shallow, the heating of the surface waters intensify and this drives the surface $f\text{CO}_2_{\text{sw}}$ to higher values. On the other hand, in the ARCT and NADR provinces, deeper MLD will result in higher $f\text{CO}_2_{\text{sw}}$ values since deeper waters are transported upwards which have higher $f\text{CO}_2_{\text{sw}}$ values as a result of higher respiration/photosynthesis ratios.

This mechanistic view shows that the thermodynamic control on $f\text{CO}_2_{\text{sw}}$ is often counteracted by biology and, again, this raises the question of the usefulness of satellite chlorophyll for $f\text{CO}_2_{\text{sw}}$ algorithms. This issue is discussed in more detail in section 3.6 since within this dataset the use of satellite chlorophyll was unsuccessful.

Ríos *et al.* (2005) showed a linear relationship between SST and $f\text{CO}_2_{\text{sw}}$ in the area around the Azores. They yielded a mean residual difference of $-3 \pm 7 \mu\text{atm}$ in their algorithm. This result is similar to the NADR result which employs SST and MLD data, but the NADR yields a smaller mean residual difference of ($f\text{CO}_2_{\text{sw observed}} - f\text{CO}_2_{\text{sw predicted}} =$) $-0.13 \pm 10 \mu\text{atm}$. The NADR validation data presented here which represent the overall accuracy of the algorithm are slightly higher ($-4 \pm 11 \mu\text{atm}$) than Ríos *et al.* (2005).

Lefèvre *et al.* (2004) divided their North Atlantic dataset into similar biogeochemical provinces, and they calculated the temperature normalized $p\text{CO}_2_{\text{sw}}$ from SST, longitude, latitude, and year using a multivariable linear regression method. As a result, they retrieved monthly algorithms for the three provinces. A direct comparison of their coefficients is not straightforward since they used temperature normalized $p\text{CO}_2$. Their goodness of fit in the NADR province yields higher values (average, NADR: $r^2 = 0.91$) compared with this work ($r^2 = 0.62$). It is not clear, however, how many data points were used for each month in the work by Lefèvre *et al.* (2004), which will affect the variability of the data. Their NADR province is also north of “our” NADR province, suggesting that they describe a system that is closer to the ARCT province.

In the high latitudes ($>50^\circ\text{N}$), $f\text{CO}_2_{\text{sw}}$ is also frequently retrieved from SST data, but the algorithms mostly vary with season, and more than one unique equation has been needed to reproduce the seasonal $f\text{CO}_2_{\text{sw}}$ variation. The correlation coefficient in the present ARCT algorithm is very close with the Lefèvre *et al.* (2004) values, being slightly higher (0.84 compared to 0.77). Aside from this publication, not many efforts have been reported to date that describe $f\text{CO}_2_{\text{sw}}$ algorithms in the ARCT province. Therefore, comparisons are shown with other investigations for regions near the ARCT province. In the Greenland Sea, Hood *et al.* (1999)

used temperature normalized seawater $f\text{CO}_{2\text{sw}}$ and SST to establish two algorithms, one for fall/winter and one for summer. The RMS values were similar (7-10 μatm) compared with the ARCT algorithm (algorithm/validation RMS = 10 μatm ; Table 4). The advantage of the ARCT algorithm in this work is that it is valid for the entire year and a greater area. For the northern North Atlantic, Olsen *et al.* (2003) developed a third-order polynomial using temperature normalized $f\text{CO}_{2\text{sw}}$ and SST which yielded an overall error of predicted $f\text{CO}_{2\text{sw}}$ of 10 μatm . This is equivalent to the ARCT algorithm; however, the algorithm of Olsen *et al.* (2003) is restricted to the winter. Temperature-normalized $f\text{CO}_{2\text{sw}}$ was also tested for possible algorithms in the present work, but no algorithm could be established that yielded better results than presented.

The predicted GFST $f\text{CO}_{2\text{sw}}$ data compare well in magnitude with the extensive Bermuda Atlantic Time Series (BATS) dataset. Bates *et al.* (2002) report a seasonal variability of seawater $p\text{CO}_2$ between 80-100 μatm , which matches the predictions in this work (seasonal range = 87 μatm). Using the BATS dataset, Nelson *et al.* (2001) produced seasonal $p\text{CO}_2$ algorithms for the Sargasso Sea which they extrapolated to the subtropical gyre. For summer, fall, and winter they used AVHRR temperature data in linear algorithms to predict the seawater $p\text{CO}_2$ of this region. Their RMS values retrieved from independent data varied between 11 and 14 μatm . This is slightly higher than the GFST validation result (10 μatm); the GFST algorithm of the present work can also be applied to all seasons. The variability in seawater $f\text{CO}_{2\text{sw}}$ is mostly controlled by temperature changes in this region, and satellite temperature is generally a reliable tool to predict this parameter. The addition of MLD in the North Atlantic algorithms improves $f\text{CO}_{2\text{sw}}$ predictions by introducing a parameter that plays a vital role for the $f\text{CO}_{2\text{sw}}$ variability. Gruber *et al.* (2002) showed that SST and mixed-layer depth represent key processes that affect the interannual variability of inorganic carbon concentration as shown by BATS.

5.2. Seasonal Maps of $\Delta f\text{CO}_2$ and CO_2 Flux

Seasonal maps of $\Delta f\text{CO}_2$ and CO_2 flux are shown in Figures 6 and 7. Each season comprises three months as follows: winter–January to March; spring–April to June; summer–July to September; fall–October to December. The various province-specific algorithms were used to estimate the $f\text{CO}_{2\text{sw}/2\times 2}$ which were combined with monthly averages of atmospheric flask measurements, AVHRR SST, and QuikSCAT wind speed data to compute the sea-air CO_2 flux on a $2^\circ \times 2^\circ$ resolution as described in sections 3.3 and Table 2.

In the ARCT province, the predicted sea-air gradient is positive in winter (average = +5 μatm ; Figure 6) and most negative during the summer (July to September: average = -33 μatm). Overall, the $\Delta f\text{CO}_2$ shows a seasonal range of 38 μatm . The wind speed based on the $2^\circ \times 2^\circ$ QuikSCAT data shows a summer minimum and winter maximum of 8 and 12 m s^{-1} , respectively, with an annual average of $10 \pm 2 \text{ m s}^{-1}$. In this northernmost province, the oceanic CO_2 uptake ($F_{2\times 2}$) is most negative (= uptake) in the spring (average = -2.7 $\text{mol m}^{-2} \text{ yr}^{-1}$) and slightly positive in winter (average: +0.7 $\text{mol m}^{-2} \text{ yr}^{-1}$; Figure 7). The seasonality compares well with earlier publications with the most negative carbon fluxes in spring (Hood *et al.*, 1999: January to March: -5 $\text{mol m}^{-2} \text{ yr}^{-1}$) and most positive in winter (Hood *et al.*, 1999: October to December: -2 $\text{mol m}^{-2} \text{ yr}^{-1}$), respectively. The fact that the Hood *et al.* (1999) estimate yields a net winter uptake, while the ARCT estimate yields an evasion is, most likely, related to regional differences. Their work was for the Greenland Sea which is much farther north than the ARCT province.

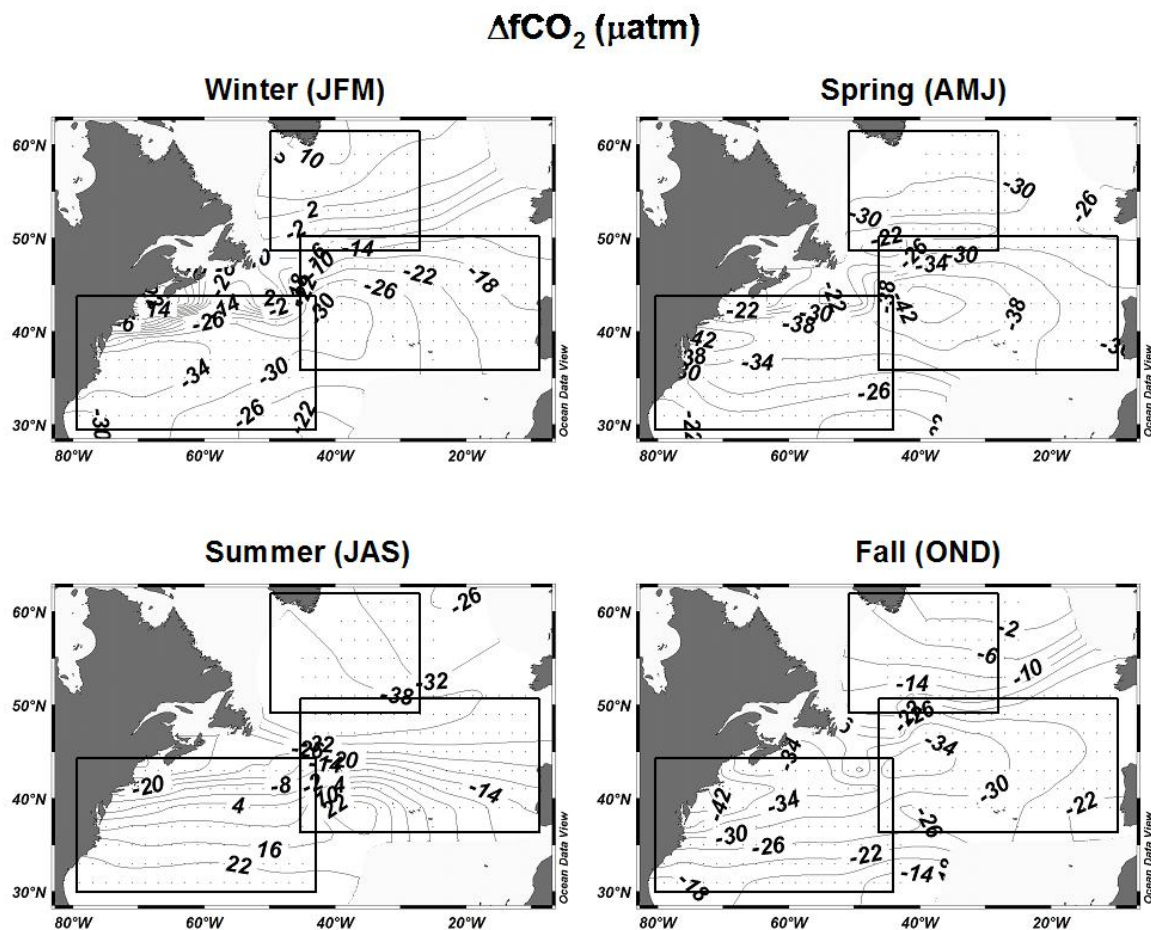


Figure 6: Seasonal $\Delta f\text{CO}_2$ across the North Atlantic. The $\Delta f\text{CO}_2$ data were calculated from the $2^\circ \times 2^\circ$ dataset which uses province-specific algorithms to predict the seawater $f\text{CO}_2$. The rectangles show the province-specific margins.

The NADR region shows a different $\Delta f\text{CO}_2$ pattern compared with the ARCT province. The $\Delta f\text{CO}_2$ is most negative in spring (average = $-33 \mu\text{atm}$; Figure 6), and this can be attributed to typical seasonal variability in this region of the North Atlantic where the carbon drawdown occurs with the onset of the spring bloom. The seasonal range is only one-third of that of the ARCT province: around $13 \mu\text{atm}$. The highest $f\text{CO}_{2\text{sw}}$ values and most positive $\Delta f\text{CO}_2$ occur during summer which is mainly caused by the thermodynamic effect of SST increase. In concert with this, Cooper *et al.* (1998) found the highest seawater $p\text{CO}_2$ values during summer in the same region. Lefèvre *et al.* (2004) calculated a mean annual $p\text{CO}_2$ of about $335 \mu\text{atm}$ for the NADR province in 1998. Assuming an annual increase in surface seawater $p\text{CO}_2$ of $1.6 \mu\text{atm}$, this corresponds to a value of around $341 \mu\text{atm}$ in 2002 and matches exactly the annual mean seawater $f\text{CO}_{2\text{sw}}$ calculated for the NADR ($341 \pm 14 \mu\text{atm}$) in 2002. The wind speed and the SST are both intermediate between the ARCT and GFST regions. The seasonal wind speed range ($4\text{-}15 \text{ m s}^{-1}$) is greater than for the other two provinces and is, on average, $9 \pm 2 \text{ m s}^{-1}$. The uptake of atmospheric CO_2 is largest in the fall (October to December = $-3 \text{ mol m}^{-2} \text{ yr}^{-1}$) and smallest in summer (July to September = $-1 \text{ mol m}^{-2} \text{ yr}^{-1}$; Figure 7).

CO₂ flux (mol m⁻² yr⁻¹)

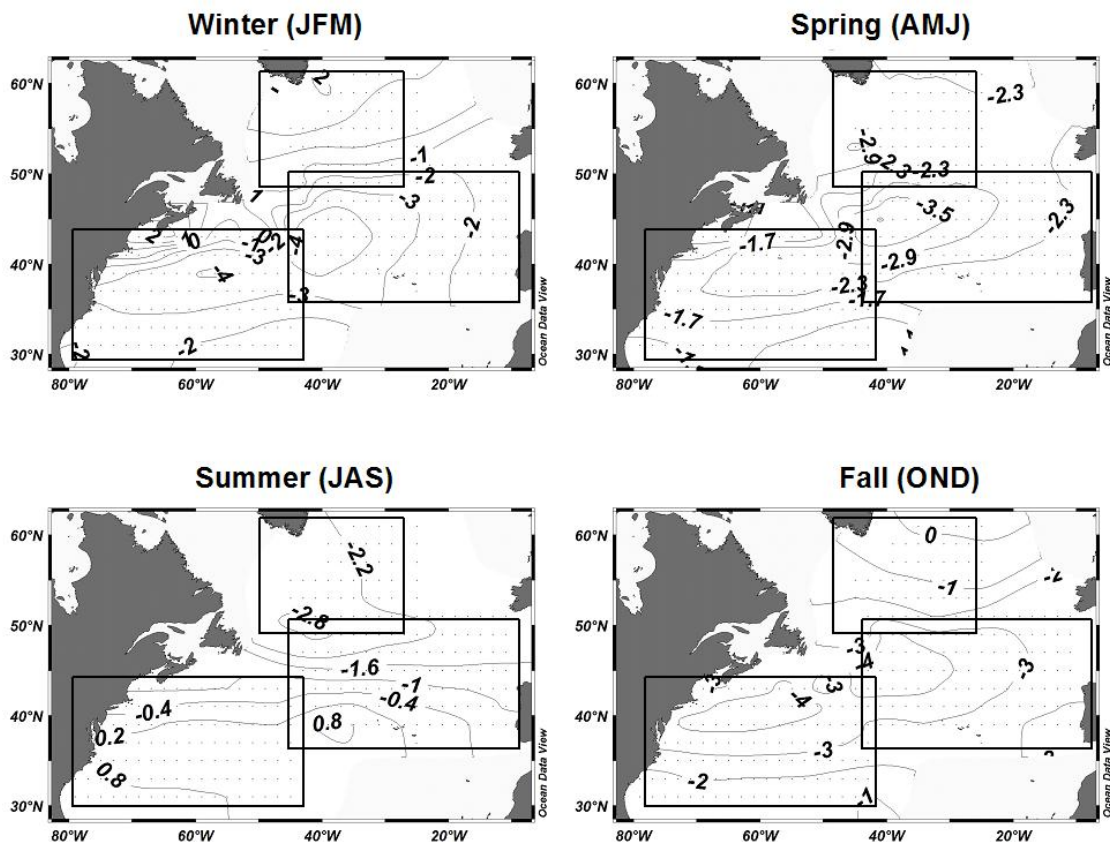


Figure 7: Seasonal CO₂ fluxes across the North Atlantic in 2002. The fluxes were calculated from the 2° × 2° dataset which uses province-specific algorithms to predict the seawater fCO₂. The rectangles show the province-specific margins.

In the GFST province, the $\Delta f\text{CO}_2$ shows a similar seasonal range as the ARCT region (37 μatm ; Figure 6). The average $\Delta f\text{CO}_2$ is always negative except during summer (July to September: +7 μatm). In winter, spring, and fall, the average $\Delta f\text{CO}_2$ is -26 μatm , -30 μatm , and -28 μatm , respectively. The sea-air CO₂ flux is close to neutral during summer (July to September = 0.2 mol m⁻² yr⁻¹) and into the ocean for the remainder of the year (October to June: -2 mol m⁻² yr⁻¹; Figure 7). The GFST province shows characteristics of the subtropical gyre which is often reported to be a weak CO₂ source (Nelson *et al.*, 2001; Takahashi *et al.*, 2002). In contrast, we find this province to be a weak sink with an annual uptake of -0.2 mol m⁻² yr⁻¹.

5.3. Source and Sink Patterns of CO₂ in the North Atlantic Ocean based on the Different Approaches

The original cruise data were bin-averaged to a 4° × 5° grid and used for CO₂ flux calculations to compare these fluxes to the 2° × 2° fluxes retrieved from the algorithms (= proxy data). Takahashi *et al.* (2002) compiled a pCO₂ climatology for the year 1995 at a 4° × 5° resolution, and their data were also used in the CO₂ flux comparison. The calculation schemes are elaborated in sections 3.3-3.5, and the data sources are described in Table 2.

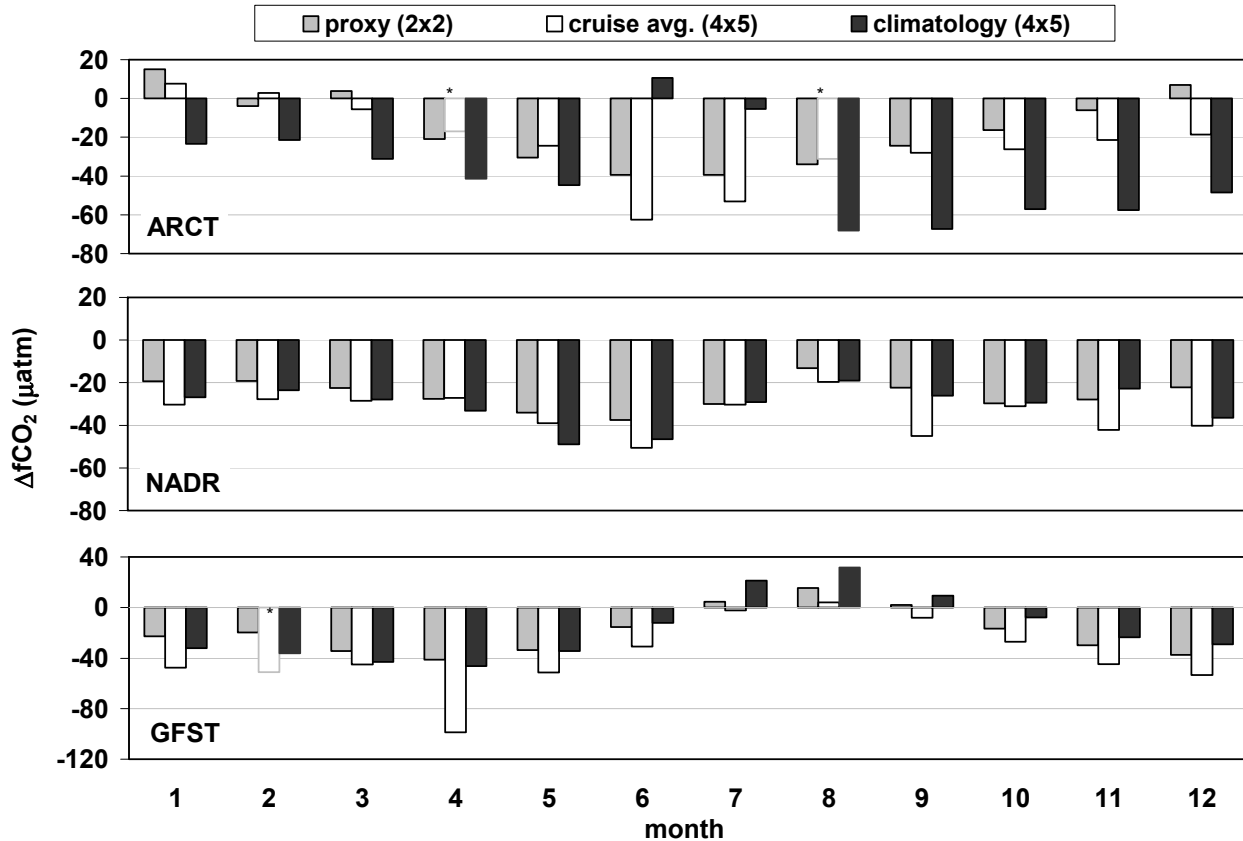


Figure 8: Comparison of the monthly $\Delta f\text{CO}_2$ within all three provinces using the $2^\circ \times 2^\circ$ proxy algorithm CO_2 (light gray), $4^\circ \times 5^\circ$ bin averaged cruise (white), and $4^\circ \times 5^\circ$ climatological (black) $f\text{CO}_2$ data within the three provinces.

The sea-air gradient resulting from the proxy estimate was on average $-20 \pm 16 \mu\text{atm}$ averaged over all three provinces (based on monthly data; Figure 8). The cruise and climatology estimates ($-32 \mu\text{atm}$ and $-29 \mu\text{atm}$, respectively) were more negative than the proxy data ($-20 \mu\text{atm}$). Specifically, for the NADR, both the climatology and cruise data yielded more negative $\Delta f\text{CO}_2$ (annual average = $-31 \mu\text{atm}$ and $-34 \mu\text{atm}$, respectively) than the proxy estimate ($-25 \mu\text{atm}$). In the ARCT province, the annual average climatological sea-air gradient was significantly more negative than the proxy and the cruise estimate ($-38 \mu\text{atm}$ compared with $-16 \mu\text{atm}$ and $-23 \mu\text{atm}$). This pattern is reversed in the GFST province where the cruise estimate is the most negative, $-38 \mu\text{atm}$, compared with $-19 \mu\text{atm}$ for the proxy data and $-17 \mu\text{atm}$ for the climatological data.

This part of the North Atlantic acted as a sink in 2002, and the ocean uptake of atmospheric CO_2 was normally lower during the summer months compared with the rest of the year (Figure 9). The proxy CO_2 flux into the ocean for all three provinces was $1.9 \text{ mol C m}^{-2} \text{ yr}^{-1}$ ($F_{2 \times 2}$). The carbon uptake estimates for the cruise averages ($F_{4 \times 5} = 3.0 \text{ mol C m}^{-2} \text{ yr}^{-1}$) and climatology ($F_{4 \times 5 \text{ climatol}} = 2.5 \text{ mol C m}^{-2} \text{ yr}^{-1}$) yield similar results and present an increased carbon sink compared with the proxy approach.

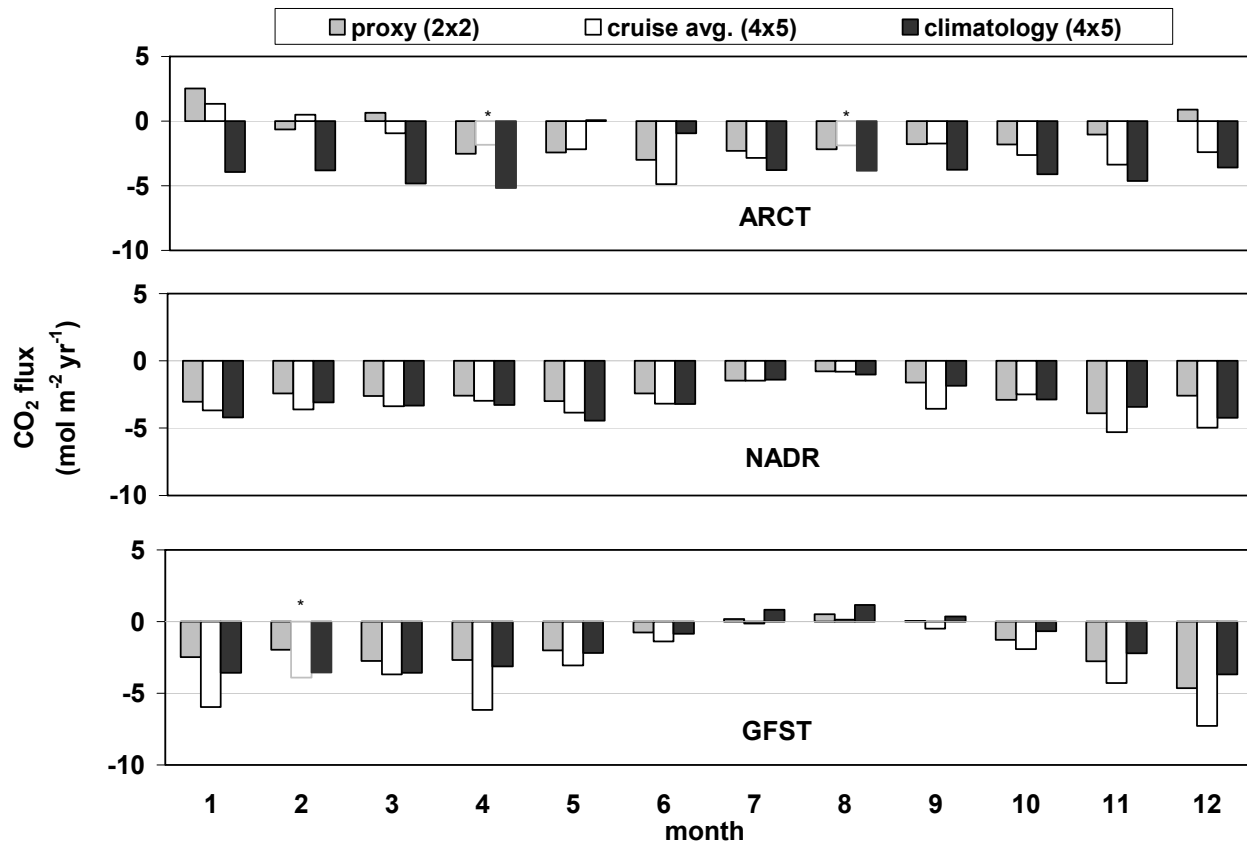


Figure 9: Comparison of the monthly CO₂ fluxes within all three provinces using the 2° × 2° proxy CO₂ (light gray), 4° × 5° bin-averaged cruise (white), and 4° × 5° climatological (black) fCO₂ data within the three provinces.

Regionally, the annual uptake rate in the ARCT province estimated from the proxy data (0.030 Pg C yr⁻¹) is about 40% lower than the cruise averages (0.051 Pg C yr⁻¹) and 68% lower than the climatology result (0.094 Pg C yr⁻¹; Table 5). The reason for the large flux difference between the climatology and proxy data must be the large differences in seawater fCO_{2,sw} since SST and SSS ranges are nearly identical. In January, for instance, the fCO_{2,sw} of both the original cruise data and the proxy data are significantly higher than the climatological data. Only one cruise (SKO 416; n = 683) was available during this time, and the fCO_{2,sw} data for the cruise averages and the algorithm approach were, on average, around 385 ± 8 μatm and 388 ± 5 μatm, respectively. The climatological fCO_{2,sw} data were much lower, on average 343 ± 12 μatm in January, which explains the flux discrepancy. The difference between the climatology and the other approaches in the ARCT fCO_{2,sw} is most likely caused by the time-dependent correction. Recent observations have shown that the surface seawater fCO₂ in the northern North Atlantic has increased at a rate slightly greater than the atmosphere over the last decades (Lefèvre *et al.*, 2004; Friis *et al.*, 2005; Omar and Olsen, 2006; Olsen *et al.*, 2006). This may be a result of lateral advection of waters loaded with anthropogenic CO₂ from farther south (Olsen *et al.*, 2006; Anderson and Olsen, 2002; Álvarez *et al.*, 2003; Macdonald *et al.*, 2003; Rosón *et al.*, 2003).

Table 5: Annual CO₂ flux calculated from three approaches for the year 2002. CO₂ proxy: algorithms have been used to calculate the flux at a 2° x 2° resolution (F_{2x2}); cruise extrapolation: all VOS cruises were bin averaged to a 4° x 5° grid and then the flux was calculated (F_{4x5}); Takahashi *et al.* (2002): climatological ΔfCO₂ were used for the flux calculation based on the 4° x 5° grids (F_{4x5/climatology}). The details of the flux calculation are described in the text.

Province	Area	CO ₂ Proxy F _{2x2}	Cruise Extrapolation F _{4x5}	Takahashi <i>et al.</i> (2002) F _{4x5/climatology}	Unit
ARCT	2.20 x 10 ¹² m ²	-0.03	-0.05	-0.09	Pg C yr ⁻¹
		-1.1	-1.9	-3.5	mol m ⁻² yr ⁻¹
NADR	6.14 x 10 ¹² m ²	-0.18	-0.24	-0.22	Pg C yr ⁻¹
		-2.4	-3.3	-3.0	mol m ⁻² yr ⁻¹
GFST	8.13 x 10 ¹² m ²	-0.17	-0.31	-0.17	Pg C yr ⁻¹
		-1.7	-3.2	-1.8	mol m ⁻² yr ⁻¹

These observations stand in contrast with Takahashi *et al.* (2002) who assume a more negative air-sea gradient with time in the area north of 45°N. In their normalization scheme to a common year, Takahashi *et al.* (2002) applied no corrections of fCO₂_{sw} data in this region. The ARCT province considered in the current work is located between 52°-63°N, and it is no surprise that the carbon uptake calculated from the climatological data is higher than the cruise averages or proxy data considering the previous assumptions. Correcting the climatological ΔfCO₂ values by adding (7·1.6 =) 11.2 μatm leads to a 30% decrease in carbon uptake (0.060 Pg C yr⁻¹) which compares well with the cruise averages, but is still twice as much as the proxy data (Table 5). Omar *et al.* (2003) compared fCO₂_{sw} data in the Barents Sea over a 33-year period and found that the sea-air gradient had stayed constant in contrast with the Takahashi *et al.* (2002) assumption. While the climatology data may be close to data for 2002 in most of the oceanic regions studied, they cannot be used for the northern North Atlantic.

In the NADR province, the annual proxy flux into the ocean is -0.18 Pg C yr⁻¹ and the differences between the proxy data, cruise averages, and the climatology are smallest (Table 5; between 19 and 25%). These uptake estimates are significantly higher than those of Ríos *et al.* (2005) who calculated an annual carbon flux into the ocean of around -0.02 Pg C yr⁻¹. However, the area chosen by Ríos *et al.* (2005) was between 34°-38°N and, therefore, only one-third of the area considered for the NADR province in this work. González Dávila *et al.* (2005) estimated a similar carbon flux for the northeast Atlantic Ocean (-0.01 Pg C yr⁻¹). This estimate is for the region around the Canary Islands and more southerly than the NADR region. It is very likely that both Ríos *et al.* (2005) and González Dávila *et al.* (2005) describe a subtropical system that is more temperature controlled and, therefore, a weaker sink compared with the NADR.

The GFST region yields an annual proxy CO₂ flux (-0.17 Pg C yr⁻¹) that is nearly twice as large as the cruise average (-0.31 Pg C yr⁻¹), but, on the other hand, it is identical with the climatology average (-0.17 Pg C yr⁻¹; Table 5). The discrepancy between the proxy and the

cruise data results are mainly from differences in SST. In December, for example, the monthly AVHRR SST used in the proxy approach is 17°C, whereas it is higher in the cruise averages (TSG SST: 21°C). Since the GFST algorithm is based on negative SST coefficients (equation 10), less negative $\Delta f\text{CO}_2$ values were returned which, in turn, decreased the oceanic CO_2 uptake. Overall, the annual carbon fluxes based on proxy data and climatology compare fairly well with earlier publications. Bates *et al.* (2001) showed that in the subtropical gyre the annual carbon sink varied between 0.03 and 0.24 Pg C yr⁻¹ for the period between 1988 and 2001. Since the carbon uptake rate from the cruise averages is significantly higher than the other two estimates, this suggests that flux estimates based on algorithms or climatology (south of 45°N) may be more accurate.

6. Conclusions

To obtain a regional CO_2 flux estimate with a precision of 0.1 Pg C yr⁻¹ in the North Atlantic Ocean, the $\Delta f\text{CO}_2$ error margins should not exceed 5 μatm between 0°-54°N, whereas it should be less than 11 μatm for the region north of 54°N (Sweeney *et al.*, 2002). This precision is difficult to obtain with the current spatial and temporal coverage of observations. Creating proxy data of higher resolution is a method to circumvent the sparsity of $f\text{CO}_{2\text{sw}}$ data. The precision of the algorithm developed for the ARCT matches the recommendation of Sweeney *et al.* (2002), whereas the precision of the NADR and GFST algorithms is about half the recommendation.

The North Atlantic Ocean is a region of high $f\text{CO}_{2\text{sw}}$ variability, and the production of spatio-temporal CO_2 flux maps of fine resolution requires an understanding of underlying mechanisms that steer the surface variables. Dividing the ocean into biogeochemical provinces facilitates this approach and increases the accuracy of algorithms that employ different parameterizations. In this work, proxy CO_2 fluxes are retrieved from satellite and real-time data that are of higher resolution than climatological data. Temperature, along with mixed layer depth, was the best tool to describe the regional variability of the CO_2 flux. Inclusion of satellite chlorophyll data did not improve the algorithms.

Flux comparisons reveal that carbon uptake estimates which are based on $f\text{CO}_{2\text{sw}}$ algorithms are lower than cruise or climatology estimates. It seems that especially in highly variable regions, for instance, the ARCT province, climatological or observational CO_2 flux estimates may overestimate the oceanic carbon uptake. In regions south of 45°-50°N, proxy and climatological data show reasonable agreement of CO_2 fluxes. In the present work, it is recommended to use proxy data to estimate the oceanic carbon uptake rather than the limited observations. The latter generally tends to overestimate the carbon uptake by exaggerating seasonal anomalies when extrapolated to a broader spatio-temporal extent.

At this point, it is unknown how much these proxy estimates will change on a year-to-year-basis. Algorithms and correlations are prone to changes on interannual scales, and it is very likely that regular fine-tuning will be required to keep these proxy estimates up to date. With the ongoing collection of VOS and satellite data, we will be able to resolve this with more confidence and higher accuracy in future projects.

7. Acknowledgments

The authors are very grateful for support from the following people: Kevin Sullivan for retrieving the M/V *Skogafoss* data, Robert Castle for providing helpful macros, and Craig Neill for his efforts on M/V *Nuka Arctica*. Thanks to Tom Conway who provided the atmospheric flask data and to all institutions that supplied the satellite data. Thanks also to Bob Molinari and Huiquin Yang who generously provided the Argo data and data products.

This research was carried out in part under the auspices of the Cooperative Institute for Marine and Atmospheric Studies (CIMAS), a Joint Institute of the University of Miami and the National Oceanic and Atmospheric Administration (cooperative agreement #NA17RJ1226). This is a contribution to the EU IP CARBOOCEAN (Contract no. 511176-2) and to REmote Sensing Carbon UptakeE (RESCUE, project 96/05 of the Swedish National Space Board).

8. References

- Álvarez, M., A.F. Ríos, F.F. Pérez, H.L. Bryden, and G. Rosón, 2003: Transports and budgets of total inorganic carbon in the subpolar and temperate North Atlantic. *Global Biogeochem. Cycles*, 17(1):1002, doi:10.1029/2002GB001881.
- Anderson, L.A., and A. Olsen, 2002: Air-sea flux of anthropogenic carbon dioxide in the North Atlantic. *Geophys. Res. Lett.*, 29(17):1835, doi:10.1029/2002GL014820.
- Bates, N.R., 2001: Interannual variability of oceanic CO₂ and biogeochemical properties in the western North Atlantic subtropical gyre. *Deep-Sea Res., Part II*, 48(8-9):1507-1528.
- Bates, N.R., A.C. Pequignet, R.J. Johnson, and N. Gruber, 2002: A short-term sink for atmospheric CO₂ in subtropical mode water of the North Atlantic Ocean. *Nature*, 420(6915):489-493.
- Cooper, D.J., A.J. Watson, and R.D. Ling, 1998: Variation of pCO₂ along a North Atlantic shipping route (United Kingdom to the Caribbean): A year of automated observations. *Mar. Chem.*, 60(1-2):147-164.
- DOE, 1994: *Handbook of Methods for the Analysis of the Various Parameters of the Carbon Dioxide System in Sea Water*, Version 2. A.G. Dickson and C. Goyet, eds., ORNL/CDIAC-74.
- Feely, R.A., R. Wanninkhof, H.B. Milburn, C.E. Cosca, M. Stapp, and P.P. Murphy, 1998: A new automated underway system for making high precision pCO₂ measurements onboard research ships. *Anal. Chim. Acta*, 377(2-3):185-191.
- Friis, K., A. Körtzinger, J. Pätsch, and D.W.R. Wallace, 2005: On the temporal increase of anthropogenic CO₂ in the subpolar North Atlantic. *Deep-Sea Res., Part I*, 52(5):681-698.
- González Dávila, M., J.M. Santana-Casiano, L. Merlivat, L. Barbero-Muñoz, and E.V. Dafner, 2005: Fluxes of CO₂ between the atmosphere and the ocean during the POMME project in the northeast Atlantic Ocean during 2001. *J. Geophys. Res.*, 110(C7):C07S11, doi: 10.1029/2004JC002763.
- Gruber, N., C.D. Keeling, and N.R. Bates, 2002: Interannual variability in the North Atlantic Ocean carbon sink. *Science*, 298(5602):2374-2378.
- Hood, E.M., L. Merlivat, and T. Johannessen, 1999: Variations of fCO₂ and air-sea flux of CO₂ in the Greenland Sea gyre using high-frequency time series data from CARIOCA drift buoys. *J. Geophys. Res.*, 104(C9):20,571-20,583.

- Kalnay, E., M. Kanamitsu, R. Kistler, W. Collins, D. Deaven, L. Gandin, M. Iredell, S. Saha, G. White, J. Woollen, Y. Zhu, A. Leetmaa, R. Reynolds, M. Chelliah, W. Ebisuzaki, W. Higgins, J. Janowiak, K.C. Mo, C. Ropelewski, J. Wang, R. Jenne, and D. Joseph, 1996: The NCEP/NCAR 40-year reanalysis project. *Bull. Amer. Met. Soc.*, 77(3):437-471.
- Körtzinger, A., 1999: Determination of carbon dioxide partial pressure (pCO₂). In *Methods of Seawater Analysis*, K. Grasshoff, K. Kremling, and M. Ehrhardt (eds.). Verlag Chemie, Weinheim, 149-158.
- Körtzinger, A., 2003: A significant CO₂ sink in the tropical Atlantic Ocean associated with the Amazon River plume. *Geophys. Res. Lett.*, 30(24):2287, doi: 10.1029/2003GL018841.
- Krauss, W., 1986: The North Atlantic Current. *J. Geophys. Res.*, 91(4):5061-5074.
- Lefèvre, N., A.J. Watson, A. Olsen, A.F. Ríos, F.F. Pérez, and T. Johannessen, 2004: A decrease in the sink for atmospheric CO₂ in the North Atlantic. *Geophys. Res. Lett.*, 31(7):L07306, doi:10.1029/2003GL018957.
- Longhurst, A., 1995: Seasonal cycles of pelagic production and consumption. *Prog. Oceanogr.*, 36(2):77-167.
- Lueger, H., D.W.R. Wallace, A. Körtzinger, and Y. Nojiri, 2004: The pCO₂ variability in the midlatitude North Atlantic Ocean during a full annual cycle. *Global Biogeochem. Cycles*, 18(3):GB3023, 10.1029/2003GB002200.
- Macdonald, A.M., M.O. Baringer, R. Wanninkhof, K. Lee, and D.W.R. Wallace, 2003: A 1998-1992 comparison of inorganic carbon and its transport across 24.5°N in the Atlantic. *Deep-Sea Res., Part II*, 50(22-26):3041-3064.
- Nelson, N.B., N.R. Bates, D.A. Siegel, and A.F. Michaels, 2001: Spatial variability of the CO₂ sink in the Sargasso Sea. *Deep-Sea Res., Part II*, 48(8-9):1801-1821.
- Olsen, A., R.G.J. Bellerby, T. Johannessen, A.M. Omar, and I. Skjelvan, 2003: Interannual variability in the wintertime air-sea flux of carbon dioxide in the northern North Atlantic, 1981-2001. *Deep-Sea Res., Part I*, 50(10-11):1323-1338.
- Olsen, A., J.A. Triñanes, and R. Wanninkhof, 2004: Sea-air flux of CO₂ in the Caribbean Sea estimated using in situ and remote sensing data. *Remote Sens. Environ.*, 89(3):309-325.
- Olsen, A., A.M. Omar, R.G.J. Bellerby, T. Johannessen, U. Ninnemann, K.R. Brown, K.A. Olsson, J. Olafsson, G. Nondal, C. Kivimäe, S. Kringstad, C. Neill, and S. Olafsdottir, 2006: Magnitude and origin of the anthropogenic CO₂ increase and ¹³C Suess effect in the Nordic Seas since 1981. *Global Biogeochem. Cycles*, 20(3):GB3027, doi:10.1029/2005GB002669.
- Omar, A., T. Johannessen, S. Kaltin, and A. Olsen, 2003: Anthropogenic increase of oceanic pCO₂ in the Barents Sea surface water. *J. Geophys. Res.*, 108(C12):3388, doi: 10.1029/2002JC001628.

- Omar, A.M., and A. Olsen, 2006: Reconstructing the time history of the air-sea CO₂ disequilibrium and its rate of change in the eastern subpolar North Atlantic, 1972-1989. *Geophys. Res. Lett.*, 33(4):L04602, doi:10.1029/2005GL025425.
- Ono, T., T. Saino, N. Kurita, and K. Sasaki, 2004: Basin-scale extrapolation of shipboard pCO₂ data by using satellite SST and Chl a. *Internat. J. Rem. Sens.*, 25(19):3803-3815.
- Press, W.H., B.P. Flannery, S.A. Teukolsky, and W.T. Vetterling, 1986: *Numerical Recipes in C: The Art of Scientific Computing*. Cambridge University Press, 994 pp.
- Ríos, A.F., F.F. Pérez, M. Álvarez, L. Mintrop, M. González-Dávila, J.M. Santana Casiano, N. Lefèvre, and A.J. Watson, 2005: Seasonal sea surface carbon dioxide in the Azores area. *Mar. Chem.*, 96(1-2): 35-51.
- Robertson, J.E., and A.J. Watson, 1992: Thermal skin effect of the surface ocean and its implications for CO₂ uptake. *Nature*, 358(6389):738-740.
- Rosón, G., A.F. Rios, F.F. Perez, A. Lavin, and H.L. Bryden, 2003: Carbon distribution, fluxes, and budgets in the subtropical North Atlantic Ocean (24.5°N). *J. Geophys. Res.*, 108(C5):3144, doi: 10.1029/1999JC000047.
- Sweeney, C., T. Takahashi, and A. Gnanadesikan, 2002: Spatial and temporal variability of surface water pCO₂ and sampling strategies. In *Appendix D: A Large-Scale CO₂ Observing Plan: In Situ Oceans and Atmosphere (LSCOP)*. National Technical Information Service, 5285 Port Royal Road Springfield, VA 22161.
- Takahashi, T., J. Olafsson, J.G. Goddard, D.W. Chipman, and S.C. Sutherland, 1993: Seasonal variation of CO₂ and nutrients in the high-latitude surface oceans: A comparative study. *Global Biogeochem. Cycles*, 7(4):843-878.
- Takahashi, T., S.C. Sutherland, C. Sweeney, A. Poisson, N. Metzl, B. Tilbrook, N.R. Bates, R. Wanninkhof, R.A. Feely, C. Sabine, J. Olafsson, and Y. Nojiri, 2002: Global sea-air CO₂ flux based on climatological surface ocean pCO₂ and seasonal biological and temperature effects. *Deep-Sea Res., Part II*, 49(9-10):1601-1622.
- Tans, P., and T.J. Conway, 2005: Monthly atmospheric CO₂ mixing ratios from the NOAA CMDL carbon cycle cooperative global air sampling network, 1968-2002. In *Trends: A Compendium of Data on Global Change*. Carbon Dioxide Information Analysis Center, Oak Ridge National Laboratory, U.S. Department of Energy, Oak Ridge, Tennessee.
- Tomeczak, M., and J.S. Godfrey, 2003: *Regional Oceanography: An Introduction*, 2nd edition. Daya Publishing House, Delhi, 390 pp.
- Walton, C.C., W.G. Pichel, J.F. Sapper, and D.A. May, 1998: The development and operational application of nonlinear algorithms for the measurement of sea surface temperatures with the NOAA polar-orbiting environmental satellites. *J. Geophys. Res.*, 103(C12):27,999-28,012.

- Wanninkhof, R., 1992: Relationship between wind speed and gas exchange over the ocean. *J. Geophys. Res.*, 97(C5):7373-7382.
- Wanninkhof, R., S.C. Doney, T. Takahashi, and W.R. McGillis, 2002: The effect of using time-averaged winds on regional air-sea CO₂ fluxes. In *Gas Transfer at Water Surfaces*, M.A. Donelan, W.M. Drennan, E.S. Saltzman, and R. Wanninkhof (eds.). Geophys. Monogr. Series, Volume 127, 351-356.
- Watson, A.J., C. Robinson, J.E. Robinson, P.J. le B. William, and M.J.R. Fasham, 1991: Spatial variability in the sink for atmospheric carbon dioxide in the North Atlantic. *Nature*, 350(6313):50-53.
- Weiss, R.F., 1974: Carbon dioxide in water and seawater: The solubility of a non-ideal gas. *Mar. Chem.*, 2(3):203-215.
- Weiss, R.F., and B.A. Price, 1980: Nitrous oxide solubility in water and seawater. *Mar. Chem.*, 8(4):347-359.
- Weiss, R.F., R.A. Jahnke, and C.D. Keeling, 1982: Seasonal effects of temperature and salinity on the partial pressure of CO₂ in seawater. *Nature*, 300(5892):511-513.